

Submitted to ApJ

Final Masses of Giant Planets II: Jupiter Formation in a Gas-Depleted Disk

Takayuki Tanigawa

*School of Medicine, University of Occupational and Environmental Health, Kita-Kyushu,
807-8555, Japan*

t-tanigawa@med.uoeh-u.ac.jp

and

Hidekazu Tanaka

Institute of Low Temperature Science, Hokkaido University, Sapporo, 060-0819, Japan

ABSTRACT

Firstly, we study the final masses of giant planets growing in protoplanetary disks through capture of disk gas, by employing empirical formulas for the gas capture rate and a shallow disk gap model, which are both based on hydrodynamical simulations. We found that, for planets less massive than 10 Jupiter masses, their growth rates are mainly controlled by the gas supply through the global disk accretion, and the gap opening does not limit the accretion. The insufficient gas supply compared with the rapid gas capture causes a depletion of the gas surface density even at the outside of the gap, which can create a disk inner hole. Secondly, our findings are applied to the formation of our solar system. For the formation of Jupiter, a very low-mass gas disk with several Jupiter masses is required at the beginning of its gas capture because of the non-stopping capture. Such a low-mass gas disk with sufficient solid material can be formed through viscous evolution from an initially ~ 10 AU-sized compact disk. By the viscous evolution with a moderate viscosity of $\alpha \sim 10^{-3}$, most of disk gas accretes onto the sun and a widely spread low-mass gas disk remains when the solid core of Jupiter starts gas capture at $t \sim 10^7$ yrs. A very low-mass gas disk also provides a plausible path where type I and II planetary migrations are both suppressed significantly. In particular, the type II migration of Jupiter-size planets becomes inefficient because of the additional gas depletion due to the rapid gas capture by themselves.

Subject headings: planets and satellites: formation — protoplanetary disks

1. Introduction

A leading hypothesis of giant planet formation is the core instability model (Mizuno 1980; Bodenheimer & Pollack 1986; Pollack et al. 1996; Ikoma, Nakazawa, & Emori 2000; Hubickyj et al. 2005). In a protoplanetary disk, a solid protoplanet attracts the disk gas and has a proto atmosphere. When the core solid is around 10 Earth masses, atmospheric mass becomes comparable to the core mass, and the atmosphere becomes gravitationally unstable, which triggers dynamical collapse of the atmosphere to become a giant planet. Since the gas accretion of the atmosphere onto the core is in an unstable and runaway manner, the growth continues as long as gas exists around the planet.

The gas-accretion growth of a giant planet is expected to terminate when the planet creates a gap, which is a low-density annulus region along the planet orbit, by its own strong gravity when the planet becomes massive. Two well-known gap-opening conditions have been widely used: the thermal condition and the viscous condition (Lin & Papaloizou 1993; Ida & Lin 2004; Crida, Morbidelli, & Masset 2006). The thermal condition is a condition that the (specific) gravitational energy at a distance of the disk scaleheight $\sim GM_p/h$ is larger than the typical thermal energy $\sim c^2$, where G is the gravitational constant, M_p is the planet mass, h is the disk scale height, and c is the sound speed of disk gas. The viscous condition is a condition that planetary gravitational torque exerting on the gas disk is stronger than the viscous torque of the disk due to Keplerian shear motion (Lin & Papaloizou 1986). Since the thermal condition usually requires a larger planet mass for gap opening than that of the viscous condition and the required planet mass is consistent with Jupiter, the final masses of giant planets have been thought to be determined by the thermal condition.

Tanigawa & Ikoma (2007) (hereafter TI07) have constructed an analytic model for the gas accretion rate onto a planet embedded in a disk gap as a function of the planetary mass, viscosity, scale height, and unperturbed surface density. By using this, they systematically studied the long-term growth and the final masses of gas giant planets. To calculate the accretion rate, TI07 derived an analytic formula for surface density distribution in the gap region, where planet gravitational perturbation is significant. In addition to the gap formula that considers the balance between the viscous torque and the planetary gravitational torque (e.g., Lubow & D’Angelo 2006), TI07 also included the gap shallowing effect by the Rayleigh stable condition that inhibits a too steep radial gradient of surface density. The shallowing effect supplies a non-negligible amount of gas into the gap bottom, which enables the giant planet to keep on growing even after the gap opening. At the same time, TI07 also proposed that the gas accretion rate onto the planet can be limited by the disk viscous accretion rate. An insufficient gas supply by the disk accretion inevitably limits the gas accretion rate onto the planet even if the planet is capable of capturing the ambient gas at a higher rate. Such a

limited accretion rate onto a planet was also used in population synthesis calculations (e.g., Mordasini et al. 2009, 2012a). As a result, TI07 gave much larger final masses ($\gtrsim 10$ Jupiter mass at 5AU) than the traditional prediction with the thermal condition for the minimum mass solar nebula (MMSN) disk.

Recent hydrodynamic simulations have extracted an empirical formula for surface density at the bottom of gap (Duffell & MacFadyen 2013; Fung, Shi, & Chiang 2014). This formula indicates that the gap is much shallower than the traditional prediction, and is even shallower than the analytic estimate given by TI07, which includes the shallowing effect by the Rayleigh stable condition. Kanagawa et al. (2015a) analytically derived this shallow gap formula, by including the effect of density wave propagation at the gap. Such a shallow gap model maintains high accretion rates onto planets and gives much larger final masses of giant planets than the prediction by TI07, leading to a possibility that Jupiter and Saturn formed in a much lighter disk than the MMSN model.

The rapid accretion onto a planet due to a shallow gap also causes a depletion of the disk gas over a wider radial region, in addition to the narrow gap. This gas depletion may alter the type II planetary migration as well as the planet growth. Lubow & D’Angelo (2006) examined this depletion mechanism due to the gas accretion onto a planet, by using their semi-analytical model and hydro-dynamical simulations. However, their estimations might suffer from large errors since the calculation time of their hydro-dynamical simulations is less than 1/10 of the characteristic viscous evolution time. It would be valuable to examine the gas depletion due to the gas accretion onto a planet, by using an updated formula for the accretion rate with the shallow gap model.

In this study, we update the growth model of giant planets proposed by TI07, by adopting the empirical shallow gap model, and demonstrate that the termination of giant planet growth by the gap opening is much harder than expected in the traditional prediction. From this result on the growth rate, we propose that a gas depleted disk is suitable for the formation of Jupiter-sized planets. We also estimate the gas depletion due to the rapid gas accretion onto the planet using the updated formula for the accretion rate, which enables us to quantitatively discuss the inner hole and its effect on the type II planetary migration. We first describe the formulation of our model in section 2. We next show examples of evolution of gas capturing growth and final mass of the giant planets in section 3. We discuss a plausible path for formation of Jupiter in section 4. The type II migration is also discussed there. Our results are summarized in section 5.

2. Formulation

2.1. Disk model

We consider a globally evolving protoplanetary disk. The protoplanetary disk has scale-height $h = c/\Omega$, where c and Ω are the sound speed and the Keplerian angular velocity around the central star, respectively. We set temperature distribution so that $h/r = 10^{-1.5}(r/1\text{AU})^{1/4}$, where r is the distance from the star. This corresponds to the temperature profile $T \simeq 280 \text{ K } (r/1\text{AU})^{-1/2}$ for solar type stars. We use α -model for disk viscosity: $\nu = \alpha ch$, where α is a non-dimensional parameter and independent of the radius r and time (Shakura & Sunyaev 1973). For the above temperature profile, ν is proportional to r . We adopt a self-similar solution for global evolution of the protoplanetary disk (Hartmann et al. 1998; Lynden-Bell & Pringle 1974). The surface density of the solution is given by

$$\Sigma_{\text{ss}}(r, t) = \frac{M_{\text{d,ini}}}{2\pi R_{\text{o}}^2} \left(\frac{r}{R_{\text{o}}} \right)^{-1} \tilde{t}_{\text{ss}}^{-3/2} \exp \left(-\frac{r}{\tilde{t}_{\text{ss}} R_{\text{o}}} \right), \quad (1)$$

$$\tilde{t}_{\text{ss}} = \frac{t}{\tau_{\text{ss}}} + 1, \quad (2)$$

where $M_{\text{d,ini}}$ is the initial total mass of the protoplanetary disk and R_{o} is the disk outer radius at $t = 0$. Note that the initial time, $t = 0$, is set to be the onset time for the dynamical gas accretion onto the giant planet's core in our model. In Equation (2), we define $\tau_{\text{ss}} = R_{\text{o}}^2/3\nu_{\text{o}}$, where ν_{o} is the viscosity at $r = R_{\text{o}}$. The total disk mass of this model is written as

$$M_{\text{d,ss}}(t) = \int_0^\infty 2\pi r \Sigma_{\text{ss}}(r, t) dr = M_{\text{d,ini}} \tilde{t}_{\text{ss}}^{-1/2}. \quad (3)$$

This means that disk mass decreases slowly with time as $\propto t^{-1/2}$. To avoid the unrealistic long lasting disk, we introduce an additional exponential decay for the disk

$$\Sigma_{\text{un}}(r, t) = \Sigma_{\text{ss}}(r, t) \exp \left(-\frac{t}{\tau_{\text{dep}}} \right), \quad (4)$$

and the disk mass is written as a function of time: $M_{\text{d,ini}} \tilde{t}_{\text{ss}}^{-1/2} \exp(-t/\tau_{\text{dep}})$. The additional exponential decay would correspond to some other mechanisms for disk dissipation, such as photoevaporation by ultraviolet radiation from the central star or disk wind (see discussion in section 5). We use Σ_{un} as the unperturbed disk surface density in this paper.

The global disk accretion rate of the self-similar solution with the additional exponential decay at an orbital radius r is given by

$$\begin{aligned} \dot{M}_{\text{d,global}}(r, t) &= \frac{M_{\text{d,ini}}}{2\tau_{\text{ss}}} \left(1 - \frac{r}{\tilde{t}_{\text{ss}} R_{\text{o}}/2} \right) \tilde{t}_{\text{ss}}^{-3/2} \exp \left(-\frac{r}{\tilde{t}_{\text{ss}} R_{\text{o}}} \right) \exp \left(-\frac{t}{\tau_{\text{dep}}} \right) \\ &= 3\pi\nu \Sigma_{\text{un}}(r, t) \left(1 - \frac{r}{\tilde{t}_{\text{ss}} R_{\text{o}}/2} \right), \end{aligned} \quad (5)$$

where the factor $\exp(-t/\tau_{\text{dep}})$ is due to the additional exponential decay.

We put the initial total mass of the protoplanetary disk as

$$M_{\text{d,ini}} = 1.1 \times 10^{-1} f_{\Sigma,5\text{AU}} \left(\frac{R_{\text{o}}}{200\text{AU}} \right)^1 M_{\odot}, \quad (6)$$

where $f_{\Sigma,5\text{AU}}$ is a parameter and M_{\odot} is the mass of the Sun. When $f_{\Sigma,5\text{AU}} = 1$, the initial total disk mass of Equation (6) makes the initial unperturbed surface density $\Sigma_{\text{un}}(5\text{AU}, t = 0)$ equal to that of the minimum mass solar nebula model at 5AU (i.e., $1.7 \times 10^{-5} M_{\odot}/\text{AU}^2 = 1.4 \times 10^3 \text{ kg/m}^2$, Hayashi et al. 1985).

It has been reported that photoevaporation by far-ultraviolet (FUV) radiation from a central star can considerably accelerate the dispersal of the circum-stellar disk (e.g., Gorti et al. 2009). Photoevaporation by FUV mainly removes the gas at the outer disk with $\gtrsim 100\text{AU}$ and decreases the disk mass exponentially with time at a relatively early stage ($\sim 10^6\text{yr}$). However, the mass loss rate by this mechanism is still uncertain at the order-of-magnitude level (e.g. Alexander et al. 2014). In this paper, thus, we do not include the effect of photoevaporation by FUV on the disk evolution for simplicity.

2.2. A new simple model for gas accretion onto a planet

We consider a protoplanet embedded in the evolving protoplanetary disk. The protoplanet with the mass M_{p} is rotating around the central star at a distance r_{p} from the star. The planet starts dynamical gas capturing, i.e., after gravitational instability of the protoplanet atmosphere around a solid core with about 10 Earth masses (Mizuno 1980; Bodenheimer & Pollack 1986; Pollack et al. 1996; Ikoma, Nakazawa, & Emori 2000; Hubickyj et al. 2005).

We introduce a formula for gas accretion rate onto the protoplanet from the protoplanetary disk by an explicit function of parameters, which enables us to obtain time evolution of the planet mass and eventually the final mass. We basically follow the method of TI07, but we have improved some points, so we will re-summarize it below.

If sufficient gas is supplied toward the planet orbit by the disk accretion, the accretion rate onto the gas giant planet is determined by the hydrodynamics of the gas accretion flow onto the planet and denoted it by $\dot{M}_{\text{p,hydro}}$. This accretion rate is given by a product of the two quantities:

$$\dot{M}_{\text{p,hydro}} = D \Sigma_{\text{acc}}, \quad (7)$$

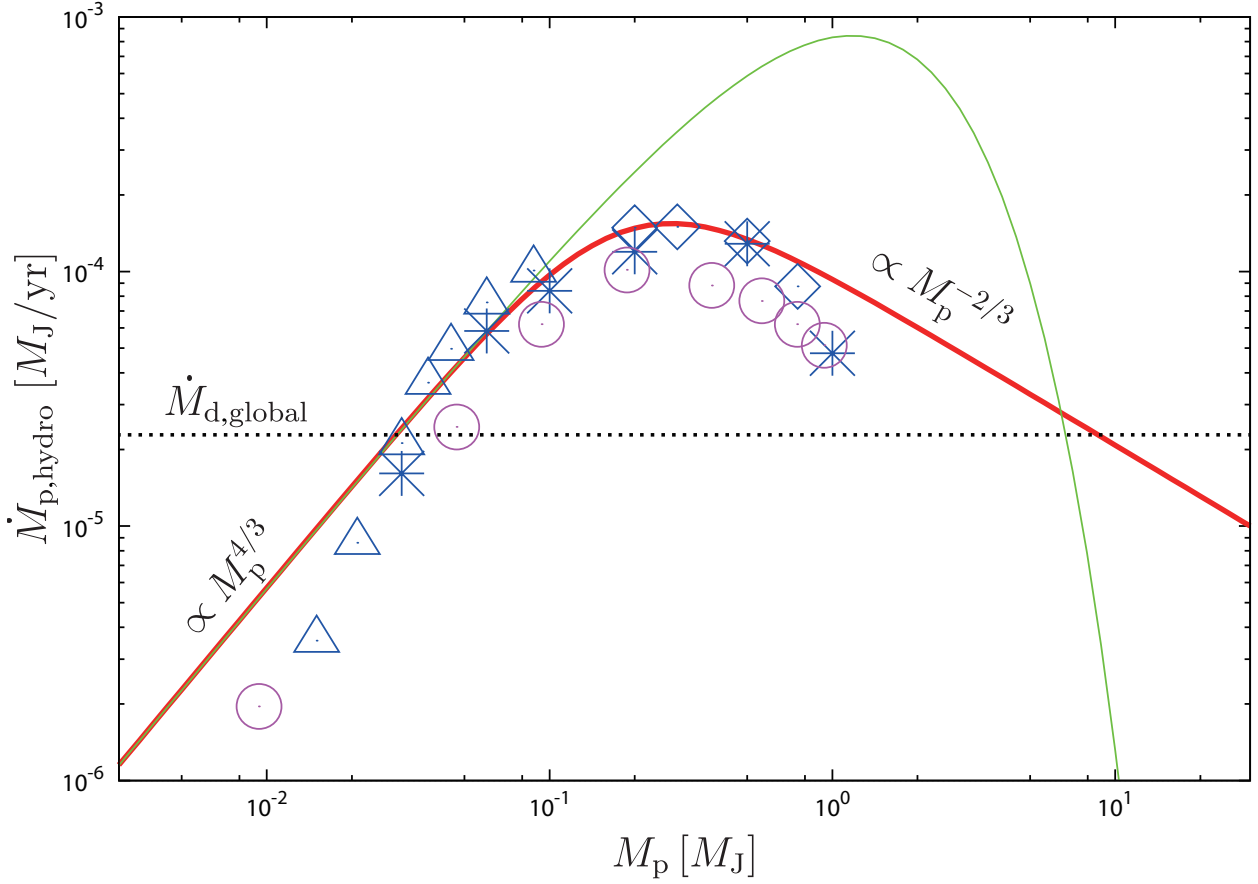


Fig. 1.— An example of gas accretion rate $\dot{M}_{p,\text{hydro}}$ as a function of planet mass when $\alpha = 4 \times 10^{-3}$, $h/r_p = 0.05$, $f_{\Sigma,5\text{AU}} = 1$ and $r_p = 5.2\text{AU}$. The red thick curve is $\dot{M}_{p,\text{hydro}}$ and the thin blue dashed curve is the corresponding accretion rate derived in Tanigawa & Ikoma (2007). The blue symbols show the accretion rates obtained by D’Angelo, Kley, & Henning (2003), where the three types of the marks correspond to different models of smoothing planet gravitational potentials. The purple circles plot the accretion rates obtained by Machida et al. (2010). As a reference, global disk accretion rate $\dot{M}_{d,\text{global}}$ is also shown.

where D is the accretion *area* of the protoplanetary disk per unit time¹, and Σ_{acc} is the surface density at the accretion channel in the protoplanetary disk. Tanigawa & Watanabe (2002) performed two-dimensional hydrodynamic simulations of the accretion flow onto a planet and derived an empirical formula for the accretion rate. According to their result, D is given by

$$D = 0.29 \left(\frac{h_p}{r_p} \right)^{-2} \left(\frac{M_p}{M_*} \right)^{4/3} r_p^2 \Omega_p, \quad (8)$$

where M_p and M_* are masses of the planet and central star, respectively, and h_p and Ω_p are scaleheight and Keplerian angular velocity at the planet location, respectively. Note that the product form of D and Σ_{acc} in Equation (7) is valid when equation of state of gas around the Hill sphere can be approximated by isothermal.

TI07 gave the formula for the surface density Σ_{acc} purely in a theoretical manner, including the Rayleigh stable condition. This condition prevents unrealistically too steep surface density gradient and resultant too deep gap, which is a consequence of the simple assumption of the balance between viscous torque and gravitational torque by the planet. However, recent hydrodynamic simulations showed that the gap is even shallower than the prediction by TI07 (Duffell & MacFadyen 2013; Fung, Shi, & Chiang 2014), which are also supported by theoretical considerations (Fung, Shi, & Chiang 2014; Kanagawa et al. 2015a,b). In this study, we thus use an empirical formula for the gas surface density at the gap bottom obtained by these studies:

$$\Sigma_{\text{acc}}(t) = \frac{1}{1 + 0.034K} \Sigma_{\text{un}}(r_p, t), \quad (9)$$

where

$$K = \left(\frac{h_p}{r_p} \right)^{-5} \left(\frac{M_p}{M_*} \right)^2 \alpha^{-1}. \quad (10)$$

In Equation (9), we assumed that the accretion band is located within the gap bottom. If the accretion band is located at the gap edge with a higher surface density, the accretion rate given by Equations (7) and (9) would be an underestimate. We set $M_{p,\text{ini}} = 3.24 \times 10^{-5} M_*$ for initial mass of the protoplanet and $R_o = 200\text{AU}$.

Figure 1 shows the accretion rate $\dot{M}_{p,\text{hydro}}$ as a function of the planet mass. In the low-mass planet case where the parameter K is much less than $1/0.034$ (~ 30), there is no gas depletion due to the gap, so Σ_{acc} can be simply replaced by Σ_{un} (see Equation (9)). The

¹ D in this paper corresponds to \dot{A} in TI07.

accretion rate in this regime is

$$\begin{aligned}\dot{M}_{\text{p,hydro}} &= \dot{M}_{\text{p,nogap}} \\ &\equiv 0.29 \left(\frac{h_{\text{p}}}{r_{\text{p}}} \right)^{-2} \left(\frac{M_{\text{p}}}{M_{*}} \right)^{4/3} \Sigma_{\text{un}} r_{\text{p}}^2 \Omega_{\text{p}} \quad \text{for } K \ll 1/0.034.\end{aligned}\quad (11)$$

In the high-mass case where $K \gg 1/0.034$, on the other hand, Σ_{acc} is reduced to $\Sigma_{\text{un}}/0.034K$ due to the gap opening and the accretion rate can be written as

$$\begin{aligned}\dot{M}_{\text{p,hydro}} &= \dot{M}_{\text{p,gap}} \\ &\equiv 8.5 \left(\frac{h_{\text{p}}}{r_{\text{p}}} \right)^1 \left(\frac{M_{\text{p}}}{M_{*}} \right)^{-2/3} \Sigma_{\text{un}} \nu_{\text{p}} \quad \text{for } K \gg 1/0.034.\end{aligned}\quad (12)$$

Equation (12) shows that the accretion rate $\dot{M}_{\text{p,hydro}}$ decreases gradually ($\propto M_{\text{p}}^{-2/3}$) after the gap opening.

In Figure 1, we also plotted the accretion rates obtained by the previous hydrodynamical simulations to check the validity of our simple model. D’Angelo, Kley, & Henning (2003) examined the gas accretion rate onto a planet embedded in a protoplanetary disk, by performing three-dimensional global hydrodynamic simulations for various planet masses. We find that our model reproduces well their results. The results of three-dimensional local simulations by (Machida et al. 2010) are also plotted and their results are in good agreement with our model². The accretion rate used in TI07 are also plotted. TI07’s accretion rate declines rapidly with increasing mass because of its deeper gap model. The global disk accretion rate $\dot{M}_{\text{d,global}}$ is also shown as a reference.

We also consider the case where the gas supply by the viscous disk accretion is insufficient. In such a case, the gas accretion onto the planet is regulated by the global disk accretion rate $\dot{M}_{\text{d,global}}(r_{\text{p}})$ rather than $\dot{M}_{\text{p,hydro}}$. We need to take into account this effect since the gap opening cannot significantly slow down the gas accretion onto the planet. Furthermore, at an early stage of the gas capture by the planet, an additional treatment is required for the realistic gas supply to the planet orbit. At the early stage, a substantial amount of gas still exists near the planet orbit. The gas supply from the nearby part is

² Machida et al. (2010) claimed that the accretion rates in two-dimensional simulations (TW02), which our model is based on in this paper, are typically two orders of magnitude larger than those in three-dimensional cases. But their fitting formula (Equation (11) for $\tilde{r}_{\text{H}}^3 < 0.3$ of their paper) is actually only a factor of 2 (or less) smaller than that in TW02 (Equation (18) of their paper). This can be confirmed by the fact that the width and position of the accretion bands in the two-dimensional (Fig. 8 of TW02) and three-dimensional (Fig. 3 of Tanigawa et al. 2012) cases are almost the same except near the midplane.

regulated by a local disk diffusion rather than the global disk accretion. The disk accretion rate due to the local diffusion is given by

$$\dot{M}_{\text{d,local}} = \pi r_{\text{p}} \Sigma_{\text{un}}(r_{\text{p}}) \sqrt{\frac{\nu_{\text{p}}}{t - t_{\text{gap}}}}, \quad (13)$$

(see Appendix A)³. In practice, the gas supply would be approximately given by the larger one of $\dot{M}_{\text{d,global}}$ and $\dot{M}_{\text{d,local}}$. In our model, therefore, by including the gas supply to the planet orbit, we give the gas accretion rate onto the planet, \dot{M}_{p} , as

$$\dot{M}_{\text{p}} = \min(\dot{M}_{\text{p,hydro}}, \max(\dot{M}_{\text{d,global}}, \dot{M}_{\text{d,local}})). \quad (14)$$

Using this model for the gas accretion rate onto the planet, we can easily simulate evolution of the planet mass (or gas accretion rate) for a given set of disk parameters. To do that, we only need to numerically integrate the ordinary differential equation because the integrand is an explicit function of the disk parameters. The final mass of a planet is simply obtained by

$$M_{\text{p,final}}(r_{\text{p}}, \alpha, h_{\text{p}}, M_{\text{d,ini}}, R_{\text{o}}) = \int_0^\infty \dot{M}_{\text{p}}(M_{\text{p}}, r_{\text{p}}, \alpha, h_{\text{p}}, M_{\text{d,ini}}, R_{\text{o}}, t) dt. \quad (15)$$

Note that Fung, Shi, & Chiang (2014) derives a more elaborate fitting formula by two-dimensional hydrodynamic simulations, which focus on cases for planets more massive than that of Duffell & MacFadyen (2013). But the difference between the two formula is much smaller than that between Duffell & MacFadyen (2013) and TI07, so we use the above equation for simplicity. In our model, we do not consider radial migration of planets, which will be discussed in Section 4.3.

³The coefficient of Equation (13) is a factor of two smaller than that in Appendix A. However this factor does not affect the final results because the accretion rate in Phase 2 (see Section 3) is not important for the final mass.

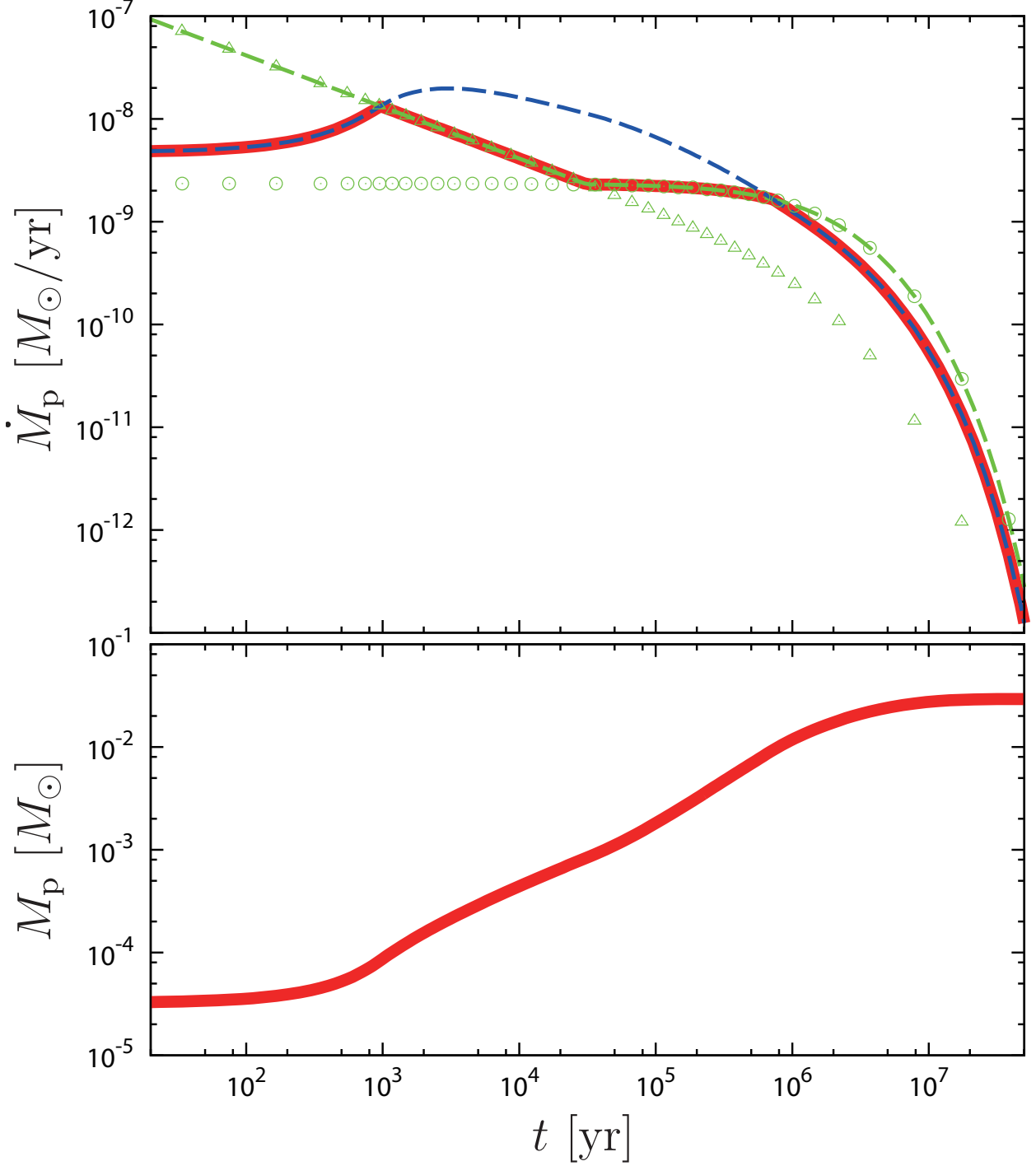


Fig. 2.— An example of time evolution for a protoplanet after the onset of dynamical gas capture in the case with $\alpha = 3.2 \times 10^{-3}$, $f_{\Sigma,5\text{AU}} = 1$, $\tau_{\text{dep}} = 10^7 \text{yr}$, $R_o = 200 \text{AU}$, $r_p = 5 \text{AU}$. Top panel shows the gas accretion rate onto the protoplanet. The thick red line shows that the accretion rate that we adopt (Equation (14)), which is a smaller one of $\dot{M}_{p,\text{hydro}}$ (blue dashed line) or $\max(\dot{M}_{d,\text{global}}, \dot{M}_{d,\text{local}})$ (green dashed line). Open circles show $\dot{M}_{d,\text{global}}$ and open triangles show $\dot{M}_{d,\text{local}}$. Bottom panel shows the mass of the protoplanet.

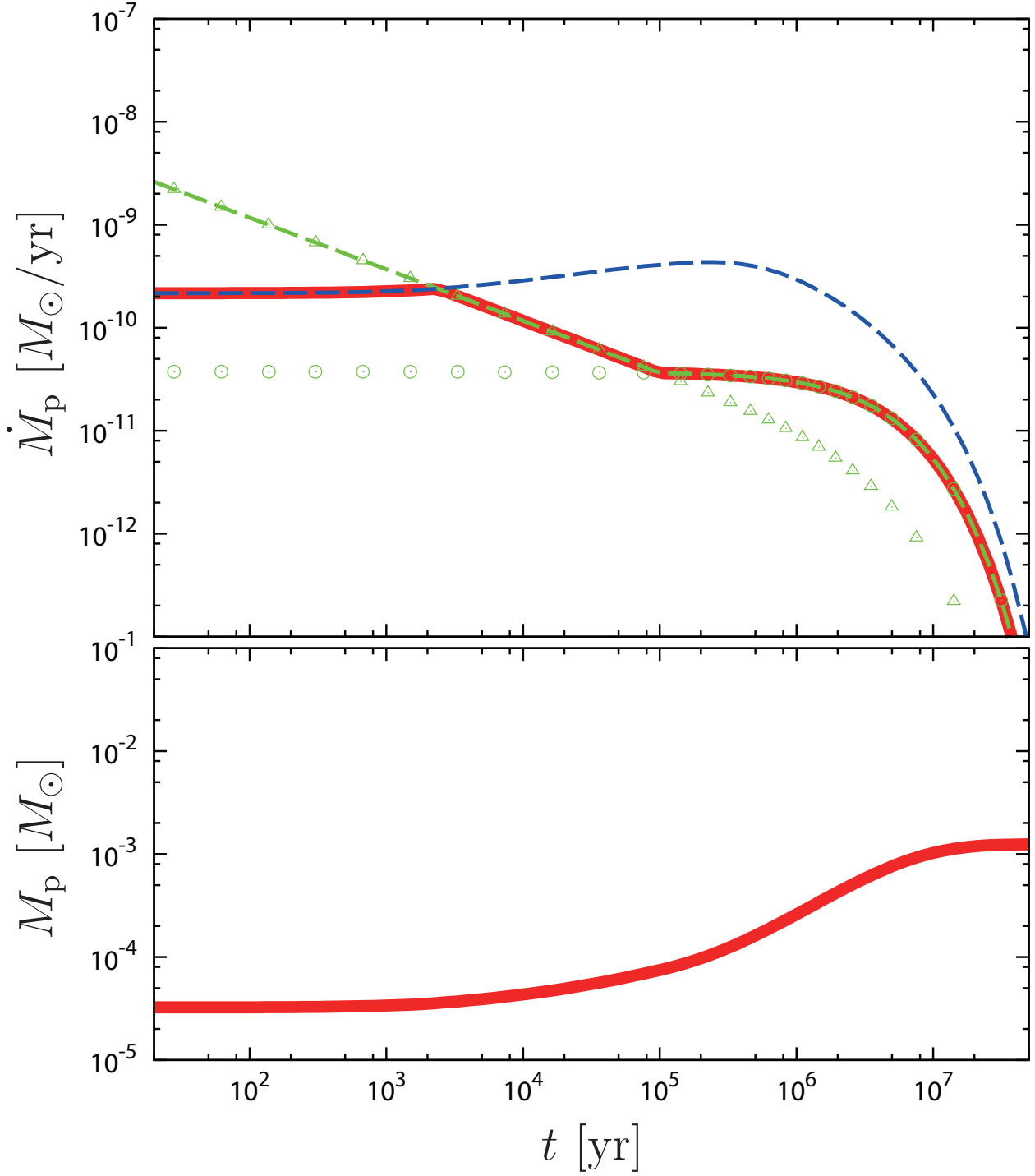


Fig. 3.— Same as Figure 2 but in the case with $\alpha = 10^{-3}$, $f_{\Sigma,5\text{AU}} = 1/20$, $\tau_{\text{dep}} = 10^7 \text{yr}$, $R_o = 200 \text{AU}$, $r_p = 5 \text{AU}$.

3. Results

3.1. Examples of time evolution

Figure 2 plots an example for time evolution of the gas accretion rate onto a proto-giant planet located at 5AU and that of planet mass. The parameters are set to be $\alpha = 3.2 \times 10^{-3}$, $f_{\Sigma,5\text{AU}} = 1$, $\tau_{\text{dep}} = 10^7 \text{yr}$, $R_o = 200\text{AU}$, $r_p = 5\text{AU}$. This example illustrates that the evolution can be divided into four phases:

- Phase 1: after the onset of dynamical gas accretion, the gas accretion rate is regulated by the hydrodynamic accretion flow without a gap: $\dot{M}_{\text{p,nogap}}$. In this case, there is abundant gas near the planet, and nothing to limit the accretion flow.
- Phase 2: the gas supply from the nearby part of the planet orbit, $\dot{M}_{\text{d,local}}$, limits the accretion rate onto the planet because it is lower than $\dot{M}_{\text{p,hydro}}$ and higher than the global disk accretion rate $\dot{M}_{\text{d,global}}$.
- Phase 3: this is also the case where the gas supply toward the planet orbit limits the accretion rate, but the rate is given by $\dot{M}_{\text{d,global}}$.
- Phase 4: this is again the case when gas supply is regulated by the hydrodynamic accretion flow, but with a deep gap: $\dot{M}_{\text{p,gap}}$.

In this case, the final mass of the giant planet is as massive as $30M_J$, which is about 1/3 of initial disk mass (see Equation (6)). The parameter set in this case is not very special (neither heavy nor highly viscous), but still results in forming a massive planet. This is because a gap does not significantly suppress gas accretion onto the planet.

The next example shown in Figure 3 is a case that produces a Jupiter-size planet. This case adopts a lower viscosity of $\alpha = 10^{-3}$ and a much lighter disk mass of $f_{\Sigma,5\text{AU}} = 1/20$. Because of the lower surface density, accretion rate in phase 1 is lower and, as a result, accretion rate and planet mass do not significantly increase until the end of phase 1. In phases 2 and 3, sequence of the phase transition is basically the same as the previous example, but the absolute values of accretion rates are reduced because of the lower surface density and lower viscosity. Accretion rates in phase 2 and 3 are proportional to $\Sigma\alpha^{1/2}$ and $\Sigma\alpha$, respectively, thus comparing with the case of Figure 2, the accretion rates in this case are reduced by factors of 36 and 60, respectively. As a result of these low accretion rates, mass of the planet does not significantly increase, and the planet is not able to open a deep gap, which leads to no emergence of phase 4. When $r_p \ll \tilde{t}_{\text{ss}}R_o/2$, we obtain from Equations (5)

and (12) as

$$\frac{\dot{M}_{\text{p,gap}}}{\dot{M}_{\text{d,global}}} \sim 0.90 \times \left(\frac{M_{\text{p}}}{M_{*}}\right)^{-2/3} \left(\frac{h_{\text{p}}}{r_{\text{p}}}\right)^1. \quad (16)$$

The emergence of phase 4 requires $\dot{M}_{\text{p,gap}} < \dot{M}_{\text{d,global}}$, which gives

$$M_{\text{p}} > 1.0 \times 10^{-2} \left(\frac{h_{\text{p}}/r_{\text{p}}}{0.05}\right)^{3/2} M_{*}, \quad (17)$$

which explains the presence or absence of phase 4 in the two cases. Thus, up to $\sim 10M_{\text{J}}$, the reduction of the accretion rate by the gap is not effective. Even in phase 4 of Figure 2, \dot{M}_{p} is not so small compared with $\dot{M}_{\text{d,global}}$ because the ratio $\dot{M}_{\text{p,gap}}/\dot{M}_{\text{d,global}}$ depends weakly on M_{p} as in Equation (16).

3.2. Final masses

Figure 4 plots the final mass of a gas-capturing planet as a function of orbital radius when $f_{\Sigma,5\text{AU}} = 1$, $\alpha = 10^{-3}$, $R_{\text{out}} = 200$ AU, $\tau_{\text{dep}} = 10^7$ yr. The solid line shows the final mass obtained in our model. We find that the final mass is 10-20 Jupiter masses in most of area and has only a slight radial dependence. Up to $\sim 10M_{\text{J}}$, a giant planet grows mostly in phase 3 and the growth rate is regulated by global disk accretion rate $\dot{M}_{\text{d,global}}$ at all radii. Thus the growth rate of giant planets is independent of their radial location. Even in phase 4 where $M_{\text{p}} \gtrsim 10M_{\text{J}}$, the growth rate is not much smaller than $\dot{M}_{\text{d,global}}$. We also plot the final mass in the case of TI07 for comparison. In the case of TI07, Σ_{acc} uses a formula of TI07, while Equation (9) is used in this paper. Final mass with TI07's formula becomes larger than Jupiter mass for most of the region. This is mainly because TI07 considers the violation of the Rayleigh condition for steep radial density gradient, which limits the gradient, tends to fill the gap, and promotes gas capturing growth as a result. In this case, the final mass of a planet increases with its orbital radius r_{p} . This is because gap opening is easier at the inner region in TI07. Thus the difference in the final mass between the two cases is originated from formulae for the gap depth.

The final mass can be estimated with a simple equation. Since the gap opening does not significantly affect \dot{M}_{p} up to $\sim 10M_{\text{J}}$, the global disk accretion rate $\dot{M}_{\text{d,global}}$ determines the final mass in most cases. Thus, using $\dot{M}_{\text{d,global}}$ for a planet at $r_{\text{p}} \ll R_{\text{o}}$, final mass is

approximated by

$$\begin{aligned}
 M_{\text{p,final,p3}} &\sim \int_0^\infty \dot{M}_{\text{d,global}} \Big|_{r_{\text{p}} \ll R_{\text{o}}} dt \\
 &\sim M_{\text{d,ini}} \left[1 - \left(\frac{\tau_{\text{dep}}}{\tau_{\text{ss}}} + 1 \right)^{-1/2} \right] = M_{\text{d,ini}} - M_{\text{d,ss}}(\tau_{\text{dep}}).
 \end{aligned} \tag{18}$$

This means that all the mass lost from the disk is captured by the planet. In the case where $\tau_{\text{dep}} \ll \tau_{\text{ss}}$, the final mass of Equation (18) is approximately given by $(\tau_{\text{dep}}/2\tau_{\text{ss}})M_{\text{d,ini}}$. When r_{p} is small, the deviation from Equation (18) becomes larger. This is because the accretion state is switched from phase 3 to 4 before the end of the growth. In this case, the final mass is roughly estimated by

$$M_{\text{p,final,p4}} \sim M_{\text{p,final,p3}} \frac{\dot{M}_{\text{p,gap}}(M_{\text{p,final,p3}})}{\dot{M}_{\text{d,global}}}. \tag{19}$$

Note that $M_{\text{d,ini}}$ is the disk mass at the time when the planet starts its gas capture and can be much smaller than the mass when the disk is formed. Time scale of global viscous evolution τ_{ss} in our fiducial case is

$$\tau_{\text{ss}} = \frac{R_{\text{o}}^2}{3\nu_{\text{o}}} = 1.1 \times 10^7 \left(\frac{\alpha}{10^{-3}} \right)^{-1} \left(\frac{h_{1\text{AU}}/1\text{AU}}{10^{-1.5}} \right)^{-2} \left(\frac{R_{\text{o}}}{200\text{AU}} \right)^1 \text{ yr}. \tag{20}$$

Figure 5 plots final masses for various initial surface densities (or disk masses). The five curves, which correspond to five $f_{\Sigma,5\text{AU}}$, show that final mass is proportional to $f_{\Sigma,5\text{AU}}$ in general. This is simply because the growth rate in phase 3 $\dot{M}_{\text{d,global}}$, which is proportional to surface density, mainly determines the final mass (see Equation (18)), and the gap effect is not significant. The final masses shown in this figure are close to possible maximum masses. In the case of Figure 5, $\tau_{\text{ss}} \simeq \tau_{\text{dep}}$, so $M_{\text{d,ini}} - M_{\text{d,ss}}(\tau_{\text{dep}}) = M_{\text{d,ini}}(1 - 1/\sqrt{2})$, which means that all the disk gas accreting inward is captured by the planet on the way toward the central star and gap has little effect on suppressing the gas capture. The final mass in the case of $f_{\Sigma,5\text{AU}} = 1$ would be about $20M_{\text{J}}$ around 5AU. For the formation of Jupiter-mass planets, the gas disk should be therefore much less massive than the MMSN disk at the onset of their gas capture.

Figure 6 plots $M_{\text{p,final}}$ as a function of r_{p} in the cases with 10 times larger and smaller values of one of the three parameters: α , τ_{dep} , and $f_{\Sigma,5\text{AU}}$. We can see that the final mass increases with both α and τ_{dep} and depends only on the product $\alpha\tau_{\text{dep}}$ in most range. For example, the degeneracy occurs at $r_{\text{p}} \lesssim 10\text{AU}$ in the cases with $(\alpha, \tau_{\text{dep}}) = (10^{-3}, 10^8)$ and $(10^{-2}, 10^7)$ or the cases of $(10^{-3}, 10^6)$ and $(10^{-4}, 10^7)$. This is because the final mass is a

function of $(\tau_{\text{dep}}/\tau_{\text{ss}})$, which is proportional to $\alpha\tau_{\text{dep}}$ (see Equation (18)). However, this dependency is weaker than that of $f_{\Sigma,5\text{AU}}$ because the dependence of final mass on $(\tau_{\text{dep}}/\tau_{\text{ss}})$ is weaker than linear (see Equation (18)), while that on $f_{\Sigma,5\text{AU}}$ is basically linear. Note that final masses for a pair of the degenerated cases ($\alpha\tau_{\text{dep}} = 10^{-3}$ or 10^{-5}) are split at $r_p \sim R_o$. This is because most of gas accretion is done by $\dot{M}_{\text{d,local}}$ (i.e., phase 2), which is proportional to $\alpha^{1/2}$, not like $\dot{M}_{\text{d,global}} \propto \alpha^1$. This situation is realized in the case when $r_p \sim R_o$ and $\tau_{\text{dep}} < \tau_{\text{ss}}$.

3.3. Gas depletion due to the accretion onto the planet

In phase 3, the disk gas is further reduced, in addition to the effect of the gap produced by the planetary torque. In this phase, the gas supply by the global disk accretion is insufficient for the rapid gas capture, which causes an additional depletion of the gas surface density even at the outside of the narrow gap region. In this phase, the accretion rate, $D\Sigma_{\text{acc}}$, cannot be larger than $\dot{M}_{\text{d,global}}$. This indicates that Σ_{acc} should be depleted because D is independent of the surface density (see Equation (7)). The additional depletion factor due to the gas capture, f' , is obtained from the balance of the mass fluxes (i.e., the mass conservation). Including this depletion factor, the disk surface density at the outside of the gap is given by $f'\Sigma_{\text{un}}(r_p)$ and, thus the hydrodynamical capture rate should be evaluated to be $f'\dot{M}_{\text{p,hydro}}$ instead of $\dot{M}_{\text{p,hydro}}$. Assuming the quasi-steady flow in the disk, we obtain an equation of the mass flux balance, $f'\dot{M}_{\text{p,hydro}} = \dot{M}_{\text{d,global}}$. Hence the additional depletion factor is given by

$$f' = \frac{\dot{M}_{\text{d,global}}}{\dot{M}_{\text{p,hydro}}} \simeq 1.1 \left(\frac{M_p}{M_*} \right)^{2/3} \left(\frac{h_p}{r_p} \right)^{-1}, \quad (21)$$

where we used Equation (16). From Equation (21), the additional depletion factor is unity for $M_p = 0.01M_*$ and 0.2 for $M_p = M_J$ in a disk with $h_p/r_p = 0.05$. Note that this additional effect of gas depletion (or enhance) does not exist in phase 4 because of sufficient supply by the global disk accretion.

Lubow & D'Angelo (2006) also examined the gas depletion due to the accretion onto the planet and derived the radial distribution of the surface density, by considering a steady viscous accretion disk with a mass sink by the planet. From this accurate surface density distribution, the additional depletion factor is given by

$$f' = \frac{\dot{M}_{\text{d,global}}}{(\dot{M}_{\text{p,hydro}} + \dot{M}_{\text{d,global}})}. \quad (22)$$

This agrees with Equation (21) when $\dot{M}_{\text{p,hydro}} \gg \dot{M}_{\text{d,global}}$. Since a detail derivation was not given in their paper, we presented the derivation of the surface density distribution in Appendix B. In Lubow & D'Angelo (2006), the ratio $\dot{M}_{\text{p,hydro}}/\dot{M}_{\text{d,global}}$ is called the accretion efficiency. They estimated the accretion efficiency from their two-dimensional hydrodynamical simulations. In Figure 7, we plot their results and our model (i.e., Equation (16)). The differences between theirs and our model are within the factor 2. Since the calculation time of their hydrodynamical simulations is less than 1/10 of the characteristic viscous evolution time, their values tends to be larger than those in the steady states. Thus we expect that the difference becomes smaller if the calculation time would be longer. Further investigation by long-term hydrodynamical simulations is necessary for checking our model.

This gas depletion would also create an inner hole, which is a depleted region inside a certain radius of a disk (e.g., Williams & Cieza 2011). Here we consider a possibility that the inner holes are formed by planets. We simply assume in Equation (21) that all the gas approaching to the planet orbit is captured by the planet when $\dot{M}_{\text{p,hydro}} > \dot{M}_{\text{d,global}}$ (i.e., in Phase 3), but Equation (22) means that all the gas is not necessarily captured even in such a case. This can be interpreted as the following. Gas capture by a planet reduces surface density in wide region, which reduces the gas capture rate in turn. When the reduced gas accretion rate is smaller than that of the global disk-viscous accretion, a fraction of gas that is not captured by the planet would need to pass through the planet orbit in a steady state. This inward flow creates a inner disk with a lower surface density, which would be a possible origin of the observed inner holes. The surface density at the inner hole would be given by $f'\Sigma_{\text{un}}(r)$, whereas we neglected this small amount of mass loss through the inner hole in phase 3 in this paper. Note that the gas depletion considered here is different from that by gap formation, which is created by gravitational torque by the planet and is usually much narrower. The gas depletion considered here is a depletion in addition to that of the gap formation. Furthermore, the gas depletion due to the gas capture also affects the type II migration of the planet. This will be discussed in detail later.

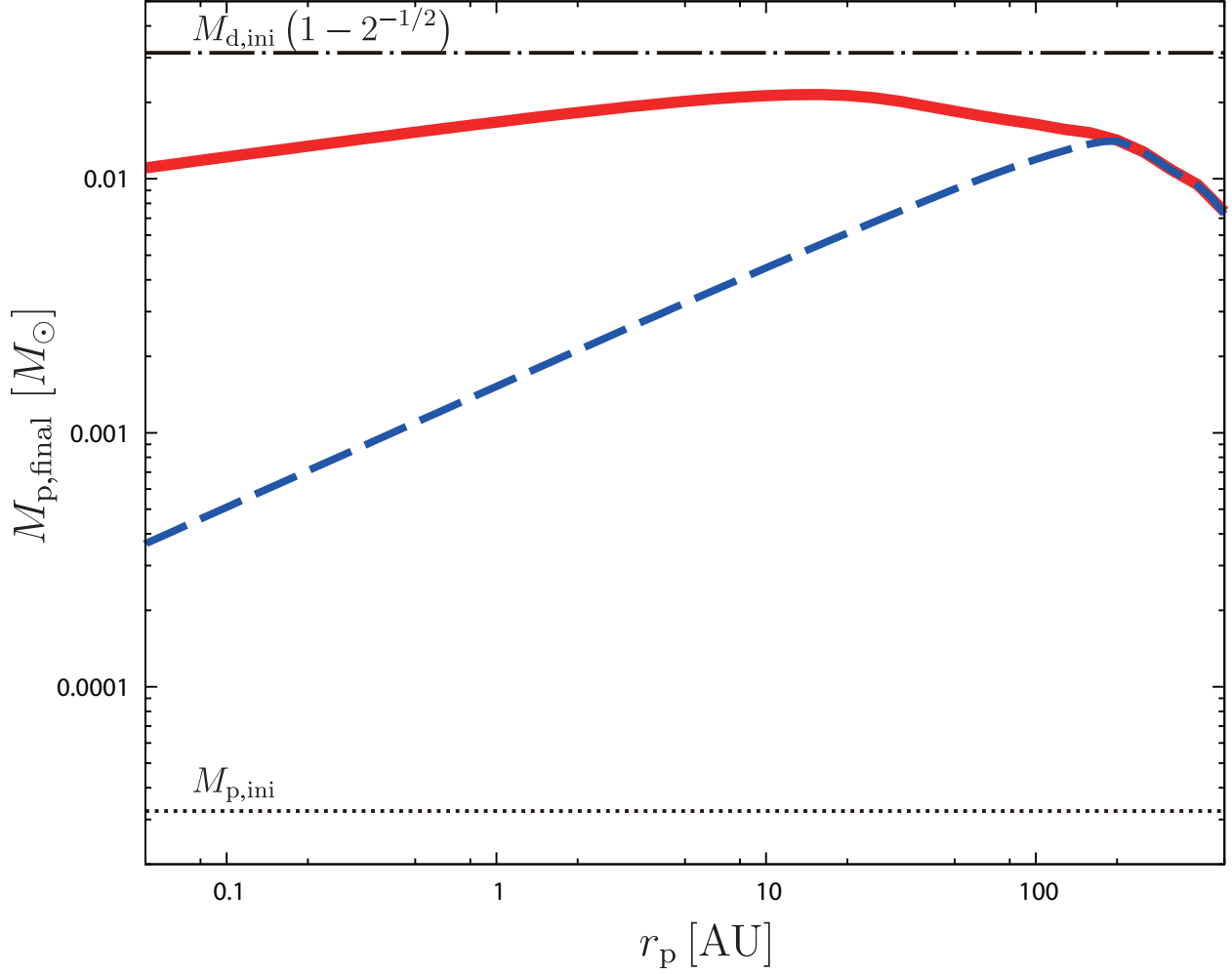


Fig. 4.— Final masses of giant planets as a function of orbital radius of the planets when $f_{\Sigma,5\text{AU}} = 1$, $\alpha = 10^{-3}$, $R_{\text{out}} = 200$ AU, $\tau_{\text{dep}} = 10^7$ yr. Red solid curves adopt the model in this paper, and the blue dashed curves shows the case when Σ_{acc} uses a formula of Tanigawa & Ikoma (2007), instead of Equation (9). The dot-dashed line corresponds to the final mass that assumes that all the gas accretion is done in phase 3 (see Equation (18)) and $\tau_{\text{dep}} = \tau_{\text{ss}}$, and the dotted line shows the initial mass of the protoplanet $M_{p,ini}$.

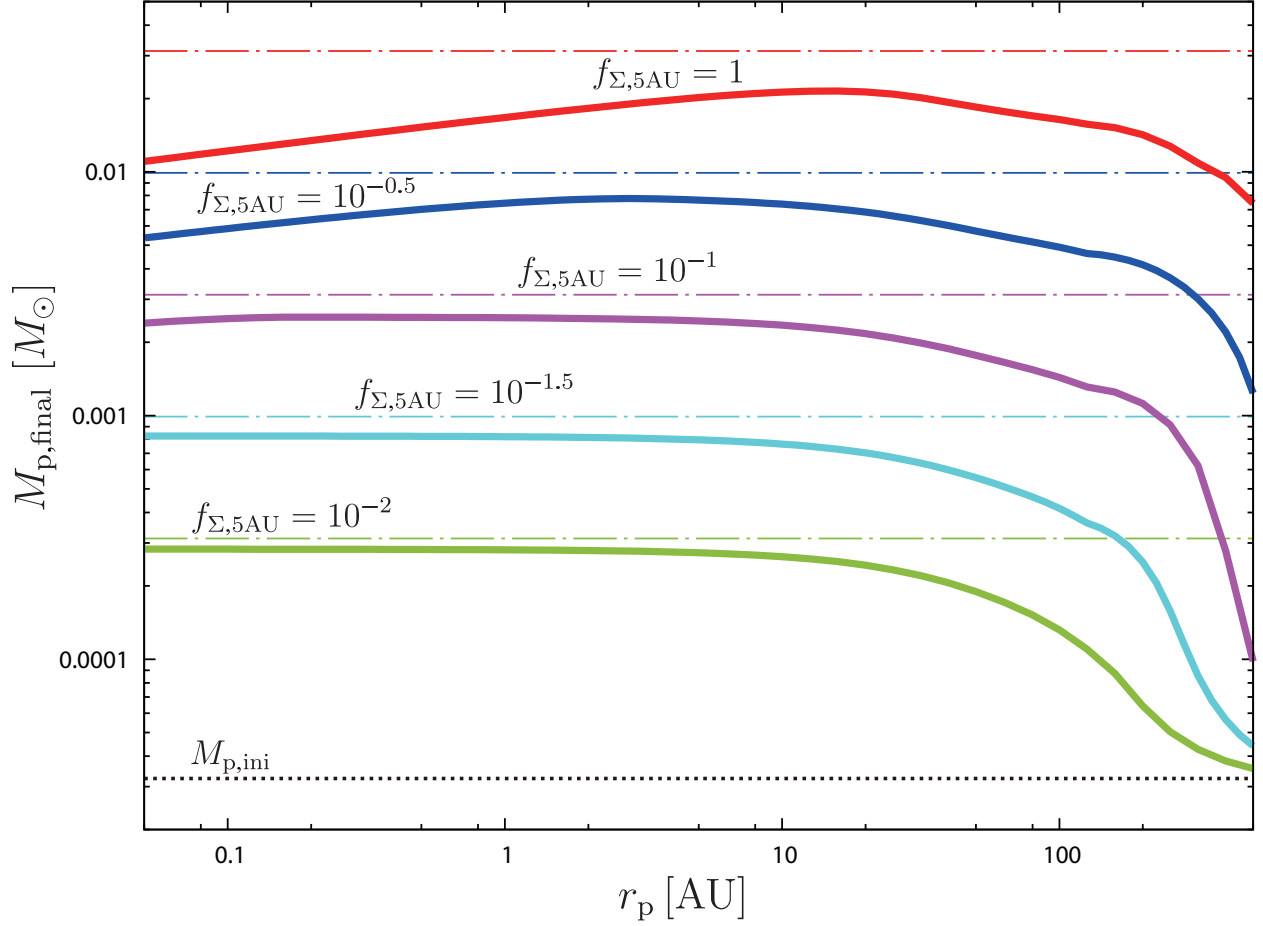


Fig. 5.— Final masses of giant planets as a function of orbital radius of the planets when $\alpha = 10^{-3}$, $R_{\text{out}} = 200$ AU, $\tau_{\text{dep}} = 10^7$ yr. Five solid curves correspond to $f_{\Sigma, 5\text{AU}} = 1, 10^{-0.5}, 10^{-1}, 10^{-1.5}, 10^{-2}$ from top to bottom, and the dot-dashed line just above the each curve is the final mass estimated by Equation (18). The dotted line shows $M_{p, \text{ini}}$.

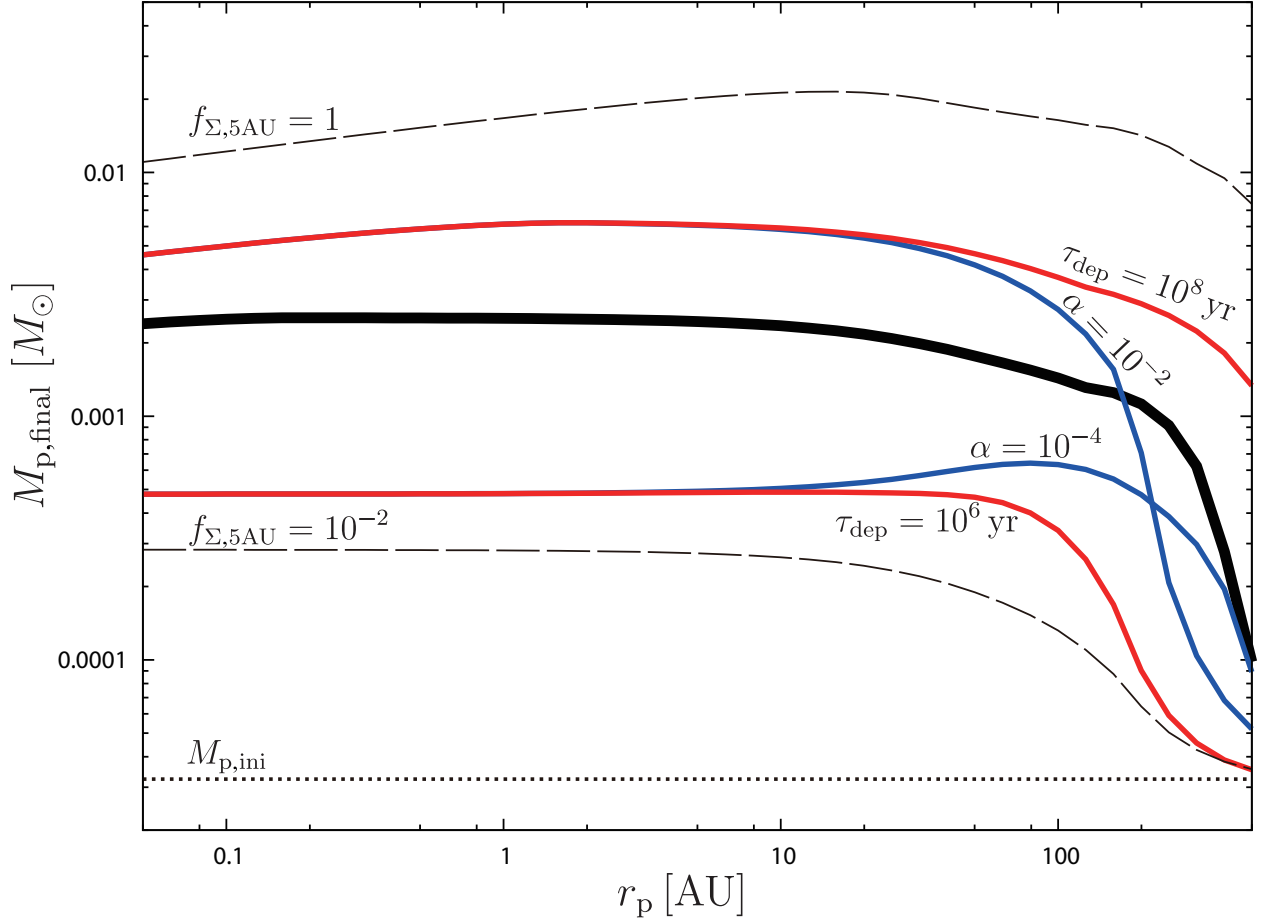


Fig. 6.— Final masses of giant planets as a function of orbital radius of the planets. The thick solid line is the same as the purple line in Figure 5 ($f_{\Sigma, 5\text{AU}} = 10^{-1}$, $\alpha = 10^{-3}$, $\tau_{\text{dep}} = 10^7 \text{ yr}$, $R_{\text{out}} = 200 \text{ AU}$). All the other lines correspond to cases with 10 times larger (or smaller) values for one of the three parameters: α , τ_{dep} , and $f_{\Sigma, 5\text{AU}}$. The two red lines show $\tau_{\text{dep}} = 10^8 \text{ yr}$ and 10^6 yr cases, the two blue lines show $\alpha = 10^{-2}$ and 10^{-4} cases, and the two thin dashed lines show $f_{\Sigma, 5\text{AU}} = 1$ and 10^{-2} cases.

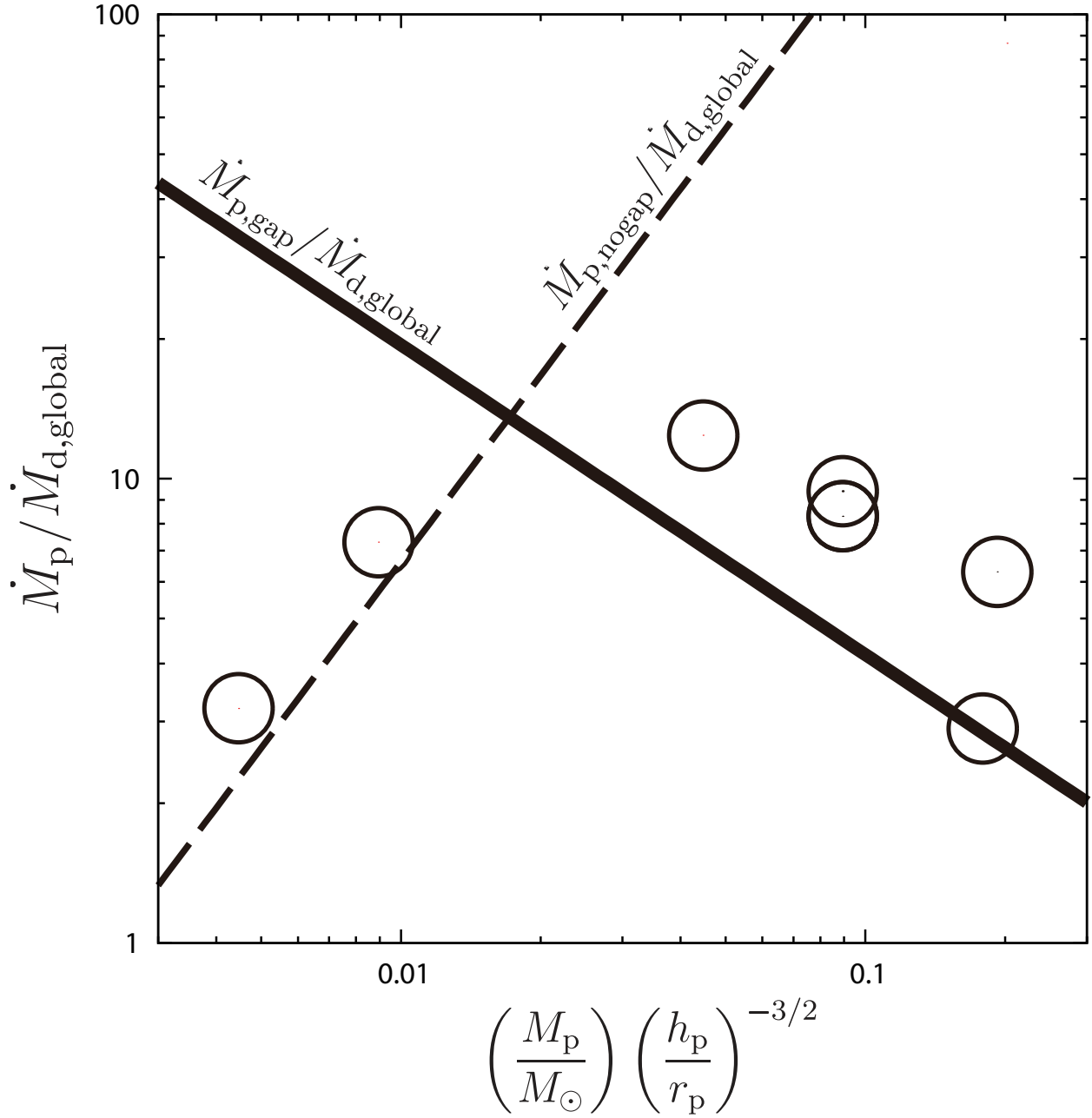


Fig. 7.— Accretion rate onto a planet normalized by disk viscous accretion rate. Circles show accretion efficiency E in Table 1 of Lubow & D'Angelo (2006), and the solid line shows $\dot{M}_{p,gap} / \dot{M}_{d,global}$. As a reference, $\dot{M}_{p,nogap} / \dot{M}_{d,global}$ is also shown by the dashed line.

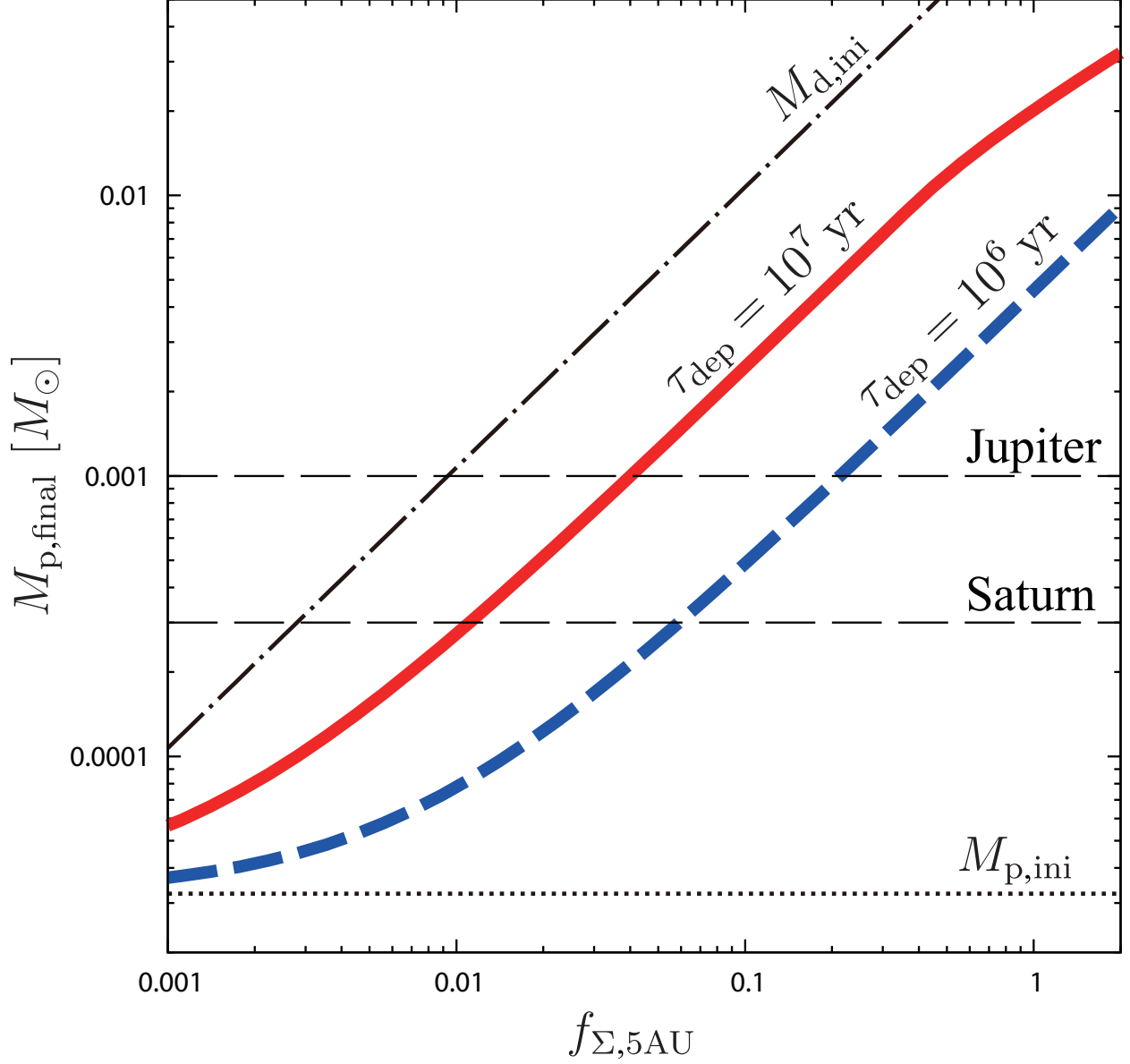


Fig. 8.— Final masses of giant planets at 5AU as a function of $f_{\Sigma,5AU}$ when $\alpha = 10^{-3}$, $R_{out} = 200$ AU in the cases of $\tau_{dep} = 10^7 \text{ yr}$ (red solid) and 10^6 yr (blue dashed), respectively. Since α and τ_{dep} is degenerated in most cases, the case with $\tau_{dep} = 10^7$ corresponds to the case with $\tau_{dep} = 10^6$ and $\alpha = 10^{-2}$, for example. The dot-dashed line shows $M_{d,ini}$, which corresponds to possible maximum mass of the planet and the dotted line shows $M_{p,ini}$.

4. Implication to the origin of our solar system

4.1. A suitable gas disk for Jupiter formation

In this paper, we updated the model for the growth of giant planets, by employing the shallow gap model revealed by the recent hydrodynamical simulations. The updated model showed that the formation of Jupiter-mass planets requires much less massive gas disks compared to the MMSN model at the stage of dynamical gas capturing by the planets. This is because the gap is not so deep to terminate the gas accretion to the planet.

Figure 8 plots $M_{\text{p,final}}$ at 5AU as a function of $f_{\Sigma,5\text{AU}}$, which indicates the depletion degree of the disk gas from the MMSN model at the beginning of the gas capture. The final mass is proportional to the depletion degree, $f_{\Sigma,5\text{AU}}$, when the final mass is much larger than the initial core mass and smaller than $10M_{\text{J}}$ (i.e., within phase 3). In the case of $\alpha = 10^{-3}$ and $\tau_{\text{dep}} = 10^7\text{yr}$, a Jupiter-mass planet is formed in a gas disk with $f_{\Sigma,5\text{AU}} = 0.04$. The total mass of this gas disk is about $4M_{\text{J}}$. Such a very low-mass gas disk also has an advantage that type I and II planetary migrations are both suppressed significantly. In a less viscous case $\alpha = 10^{-4}$ (or equivalently a short disk lifetime case $\tau_{\text{dep}} = 10^6\text{yr}$), $f_{\Sigma,5\text{AU}} = 0.3$ is suitable. However, such a moderate-mass disk does not slow down the planetary migrations significantly. Hence we adopt the former case as a suitable gas disk for Jupiter formation. If we adopt a higher viscosity $\alpha > 10^{-3}$ or a longer depletion time ($\tau_{\text{dep}} > 10^7\text{yr}$), the suitable disk mass further decreases. As mentioned in Section 3, the final mass depends on the product $\alpha\tau_{\text{dep}}$. Thus, the case of $\alpha = 3 \times 10^{-3}$ and $\tau_{\text{dep}} = 3 \times 10^6\text{yr}$ also gives a suitable disk with $f_{\Sigma,5\text{AU}} = 0.04$ as well as the former case. For the Saturn case, $f_{\Sigma,5\text{AU}}$ should be an even lighter disk (~ 0.01 when $\tau_{\text{dep}} = 10^7\text{yr}$ and $\alpha = 10^{-3}$), or later start (shorter duration) of the dynamical gas capture (ex. $f_{\Sigma,5\text{AU}} \sim 0.06$ when $\tau_{\text{dep}} = 10^6\text{yr}$).

4.2. Viscous evolution from a compact disk to a low-mass disk with high metallicity

Jupiter and Saturn have solid cores and also contains a considerable amount of heavy elements in their H/He envelopes. The two giant planets are expected to have solid components of $30\text{--}60M_{\text{E}}$ in total (e.g., Baraffe et al. (2014)). This shows that Jupiter and Saturn have much higher metallicity than the solar composition. If we also consider solids in other planets, the formation of our solar system requires solid materials of $\gtrsim 80M_{\text{E}}$ in total, which is consistent with the amount of solid included within 50AU of the MMSN disk. However, the above low-mass disk with $4M_{\text{J}}$ contains solid components of less than $20M_{\text{E}}$ if it has the solar composition, in which heavy elements are 1.4% in mass. Hence, the low-mass disk

should have very high metallicity.

A low-mass disk with high metallicity can be formed through a viscous disk evolution from a compact size described by Equation (1). Consider an initially compact disk with radius of $\sim 10\text{AU}$ and with the solar composition. The disk mass is $\sim 18M_{\text{J}}$, it thus contains solid material of $\sim 80M_{\text{E}}$. Because of the compactness, the gas and solid surface densities of this disk are twice of the MMSN model at 5AU. Firstly, planetesimals are formed in-situ and decoupled with the gaseous disk before the disk evolution. Secondly, the compact gas disk suffers a viscous accretion and losses most of gas within a relatively short time. The gas disk spreads out to $\sim 200\text{AU}$ and reduces its mass to $\sim 4M_{\text{J}}$ at $t = 10^7\text{yr}$ in the case of $\alpha = 10^{-3}$ (see Equation (20)). During the disk evolution, planetary embryos grow, and finally a sufficient large solid core causes dynamical collapse of its envelope and starts to capture its surrounding disk gas rapidly. This scenario explains the suitable low-mass disk with high metallicity for Jupiter formation in a natural way. Saturn formation would also be reasonable if the onset of dynamical gas capture occurs at even later time. It can also naturally explain the high metallicity of Jupiter and Saturn of the factor ~ 10 .

4.3. Type I and type II migration in gas-depleted disks

Here we discuss more in detail type I and type II migration in gas-depleted disks. In particular, we show below that the type II migration of Jupiter-size planets or smaller is inefficient because of the additional gas depletion due to the rapid gas capture described in Section 3.

Because of the problematic rapid type I migration (Tanaka et al. 2002), the studies on planet population synthesis prefer a gas-depleted (or high-metallicity) disk or a significant reduction of the type I migration speed (Daisaka et al. 2006; Ida & Lin 2008a; Mordasini et al. 2012b). In the gas depleted disk adopted in our scenario, the solid surface density is twice of the MMSN disk whereas the gas surface density is depleted to 4% at the end of the core-growth stage. This requires the solid-to-gas ratio to be 50 times as large as that of the solar composition. This enhancement is comparable to that required in the population synthesis calculations. Hence our scenario for Jupiter formation is a plausible and natural path which can overcome the type I migration problem. Mordasini et al. (2012c) also included the viscous disk evolution in their population synthesis calculations but they fixed the initial disk outer radius to be 30AU. Such an intermediate-size disk takes longer time to deplete the disk gas enough by disk accretion. More compact initial disks should also be examined in population synthesis calculations.

Next we examine type II migration in the gas-depleted disk. In our model of giant planet formation, we did not include the effect of type II migration. It is worthwhile to estimate the timescale of type II migration for our gas-depleted disk. Recently Duffell et al. (2014) have derived an empirical formula of migration speed in the classical type II regime from their hydrodynamical simulations and the revised timescale of type II migration is given by

$$\begin{aligned} t_{\text{migII}} &= 0.14 \frac{2r_p^2}{3\nu_p} \frac{M_p}{\Sigma_{\text{out}} r_p^2} \\ &= 0.089 \frac{M_p}{\nu_p \Sigma_{\text{out}}}, \end{aligned} \quad (23)$$

where Σ_{out} is the gas surface density outside of the gap and corresponds to $\Sigma(r_p)$ in Appendix B. Equation (23) corresponds to the “planet-dominate” case where $M_p > \Sigma_{\text{out}} r_p^2$. This condition is safely satisfied in the gas-depleted disk we consider. Equation (23) agrees well with the hydrodynamical simulations by Dürmann & Kley (2015) within a factor of ~ 2 in the “planet-dominate” case and is almost consistent with analytically derived formulae by Armitage (2007), which is used in population synthesis calculations.

As newly pointed out in this paper, for a giant planet smaller than $\sim 10M_J$, the gas surface density outside of the gap Σ_{out} suffers an additional depletion from the unperturbed disk because of the rapid gas capture by itself. The additional depletion factor f' is given by Equation (21). It gives 0.2 for Jupiter mass and $h_p/r_p = 0.05$. This additional depletion factor is derived from the mass-flux balance in the outer disk (see the subsection 3.1 and Appendix B). This effect slows down the type II migration and lengthen t_{migII} by the factor of $1/f'$. Also note that the additional depletion decreases the lower limit of M_p for the “planet-dominate” case. Any previous models of type II migration do not include the effect of this additional gas depletion. In fact, the gas capture rate, $\dot{M}_{p,\text{hydro}}$, is not taken into account in population synthesis calculations and thus they cannot evaluate this depletion factor $f' = \dot{M}_{\text{d,global}}/\dot{M}_{p,\text{hydro}}$.

The growth time of giant planets less than $\sim 10M_J$ is given by

$$t_{\text{grow}} = \frac{M_p}{\dot{M}_p} = \frac{M_p}{3\pi\nu_p\Sigma_{\text{un}}}, \quad (24)$$

which is almost equal to t_{migII} if the unperturbed surface density Σ_{un} is replaced by Σ_{out} . Hence the ratio $t_{\text{grow}}/t_{\text{migII}}$ is given by

$$\frac{t_{\text{grow}}}{t_{\text{migII}}} = f' \simeq 1.2 \times \left(\frac{M_p}{M_*}\right)^{2/3} \left(\frac{h_p}{r_p}\right)^{-1}. \quad (25)$$

This indicates the Jupiter mass or smaller planets suffer only a small radial drift by type II migration during their growth. According to our growth model, the growth of giant planets

terminates only when the disk is depleted to a negligible mass. Hence our results indicate that type II migration is ineffective for Jupiter mass planets or smaller. On the other hand, since the previous models neglect this additional gas depletion, the growth time is always comparable to t_{migII} , provided that the growth is controlled by the global disk accretion (Benz et al. 2014). Figure 9 shows growth-migration curves. Evolutions of our model shows growth without significant migration until $M_p \sim M_J$, while the case with traditional type II migration shows relatively rapid inward migration.

Calculations of planet population synthesis suggest that most giant planets fall to their host stars because of their rapid type II migration (e.g., Ida & Lin 2008b). This is inconsistent with the radial distribution of observed extra-solar planets, in which Jupiter-sized planets are piled up at $\sim 1\text{AU}$ and hot Jupiters are minor (Mayor et al. 2011; Ida et al. 2013). Hasegawa & Ida (2013) discussed possible mechanisms which slows down the type II migration but did not find any effective slowdown mechanisms. In the above and Figure 9, we showed that type II migration of giant planets smaller than $\sim 10M_J$ slows down because of the additional gas depletion due to their rapid gas capture. Our slow down mechanism may resolve the problem of type II migration.

For giant planets larger than $\sim 10M_J$ (i.e., in phase 4), the gap effect prolongs the growth time compared with Equation (24) and the additional gas depletion does not occur. Then we find that the time ratio is again given by Equation (25) but f' given by Equation (21) is larger than unity in this case. The time scale of type II migration is shorter than the growth time for $M_p > 10M_J$. This may explain that extra-solar planets more massive than $10M_J$ are observed less frequently. A detail population synthesis calculation would be necessary, including our slowdown mechanism for type II migration.

5. Summary and Discussion

We examined the growth rates and the final masses of giant planets embedded in protoplanetary disks through capture of disk gas, by employing an empirical formula for the gas capture rate and a shallow disk gap model, which are both based on hydrodynamical simulations. Our findings are summarized as follows.

1. Because of the shallow gap revealed by recent hydrodynamical simulations, giant planets do not stop their gas-capturing growth. Only the depletion of the whole gas disk can terminate their growth. For planets less massive than $10M_J$, their growth rates are mainly controlled by the gas supply through the global disk accretion, rather than their gaps. For such a mass range, the final planet mass is given by Equation (18). For

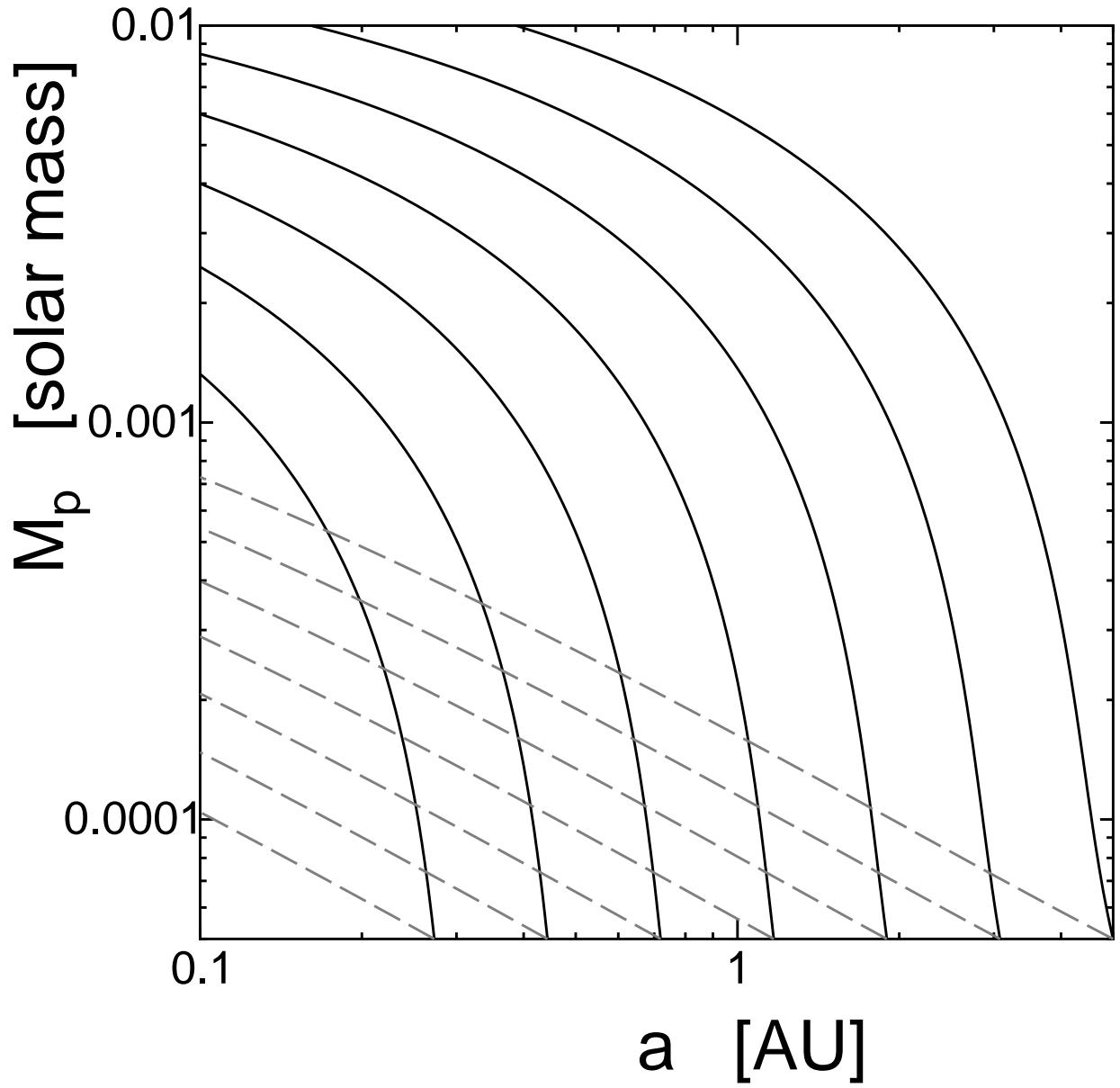


Fig. 9.— Growth-migration curves. Solid curves show evolution paths base on our result (Equation (25)), and dashed curves are the cases where the traditional type II migration is used.

the more massive planets, their growth rates are limited by deep gaps and their final mass is given by Equation (19).

2. For planets less massive than $10M_J$, the gas supply to the planets by the disk accretion is insufficient. This also causes a depletion of the gas surface density even at the outside of the gap and create an inner hole in the protoplanetary disk. The additional gas depletion factor is given by Equation (21) (see also Appendix B). Our result suggests that less massive giant planets can create deeper inner holes than more massive ones.
3. Because of the non-stopping growth, the Jupiter formation requires a very low-mass gas disk with a few or several M_J , at least, at the beginning of its gas capture. This disk is much less massive than the MMSN model, whereas the solid material of ~ 80 Earth masses is also necessary for formation of the planets in our solar system. That is, we need a very low-mass disk with a high metallicity. These requirements can be achieved by the viscous evolution from an initially ~ 10 AU-sized compact disk with the solar composition. For a disk with a moderate viscosity of $\alpha \sim 10^{-3}$, most of disk gas accretes onto the central star and a widely-spread low-mass gas disk remains at $t \sim 10^7$ yrs. This scenario can explain the high metallicity in giant planets of our solar system.
4. A very low-mass gas disk also provides a plausible path where type I and II planetary migrations are both suppressed significantly. In particular, we also showed that the type II migration of Jupiter-size planets is inefficient because of the additional gas depletion due to their rapid gas capture. This slow type II migration is consistent with the radial distribution of observed extra-solar planets in which Jupiter-sized planets are piled up at ~ 1 AU.

In this paper, we proposed the formula that describes the gas accretion rate onto the planet, which combines an empirical formula of gas accretion rate obtained by a local hydrodynamic simulation (TW02) and another empirical formula of gap depth obtained by global hydrodynamical simulation (Duffell & MacFadyen 2013). Although the accretion rate is in good agreement with global hydrodynamic simulations, the function $\dot{M}_{p, \text{hydro}}$ (or more specifically D) should be checked by making use of recent advancement of hydrodynamic simulations. We also proposed a formation of large-scale disk depletion created by gas capture of the planet based on analytic argument (see appendix B). This depletion arises also from long-term viscous evolution of the gas disk, which have not been studies so far. To check this, high-resolution hydrodynamic simulations with long-term evolution should be done in future work. Malik et al. (2015) have recently investigated the gap-opening criterion of migrating planets in protoplanetary disks and found that the gap opening is

more difficult than the traditional condition, which is based on the torque balance (e.g., Crida, Morbidelli, & Masset 2006; Lin & Papaloizou 1993). Other recent hydrodynamic simulations (Duffell & MacFadyen 2013; Fung, Shi, & Chiang 2014) also showed that the gap opening is less significant, although there are some differences on assumptions and purposes. Also, gas in the gap region tends to be turbulence by magneto-rotational instability (Gressel et al. 2013; Keith & Wardle 2015), which would lead to an even shallower gap. To quantify the gap deepening effect, further studies would be necessary.

In-situ formation of hot jupiters is thought to be difficult in general. This is because (1) a planet in inner region is easier to form a gap than that in outer region, which meant that the planet growth stops at a mass much less than that of Jupiter, (2) even if a hot jupiter forms, it is susceptible to type II migration and falls to the central star, and (3) there are not enough solid materials to trigger the dynamical gas capture of the protoplanet. Our model showed that the gap has little effect on suppressing gas accretion rate onto planets. In this sense, the first point is not a reason to prevent from in-situ formation anymore. We also showed that the type II migration is less effective than previously thought, which would not rule out the in-situ formation either. Although we have no claim that there are enough solid to form large solid cores, we should be noted that the difficulty of the in-situ formation of hot jupiters are greatly mitigated.

Our model assumes forced exponential decay with respect to time for the protoplanetary disk, but the way of disk dissipation would impact significantly on disk evolution and thus also on the planet formation scenario described above. Several mechanisms in addition to viscous disk accretion are proposed, such as photoevaporation (Hollenbach et al. 1994; Clarke et al. 2001; Owen et al. 2012), solar wind stripping (Horedt 1978; Matsuyama et al. 2009), solar wind induced accretion to the central star (Elmegreen 1978), disk wind (Suzuki & Inutsuka 2009, 2014). Among them, photoevaporation is thought to be the dominant mechanism to dissipate disks.

Photoevaporation has been actively studied recently and roles of X-ray and UV irradiation from the central star has been substantially understood. Since, however, luminosity of X-ray, EUV, and FUV and the time evolution has large uncertainty, the evolution of protoplanetary disks would have wide variety. If disk accretion rate toward the central star:

$$\dot{M}_{\text{d,global}} = 5 \times 10^{-9} f_{\Sigma,5\text{AU}} \left(\frac{\alpha}{10^{-3}} \right)^1 \left(\frac{h_{1\text{AU}}/1\text{AU}}{10^{-1.5}} \right)^2 M_{\odot}/\text{yr} \quad (26)$$

is larger than mass-loss rate by photoevaporation, the effect of photoevaporation can be neglected. Our scenario suggests that $f_{\Sigma,5\text{AU}} \sim 0.04$ is a plausible parameter, which gives $\dot{M}_{\text{d,global}} = 2 \times 10^{-10} M_{\odot}/\text{yr}$. According to Owen et al. (2012), mass-loss rate can be in a range from 10^{-12} to $10^{-7} M_{\odot}/\text{yr}$ depending on X-ray luminosity, which means that our

scenario is realized when X-ray luminosity is not strong.

We are grateful to Masahiro Ikoma, Hiroshi Kobayashi, Satoshi Okuzumi, and Kazuhiro Kanagawa for valuable comments. This work was supported by JSPS KAKENHI Grant Numbers 24103503, 26800229, 15H02065, 26287101.

A. Derivation of Equation (13)

The diffusion equation of surface density $\Sigma(r, t)$ in a Keplerian disk with viscosity ν is

$$\frac{\partial \Sigma}{\partial t} = \frac{3}{r} \frac{\partial}{\partial r} \left[r^{1/2} \frac{\partial}{\partial r} (\Sigma \nu r^{1/2}) \right]. \quad (\text{A1})$$

Adopting the local approximation ($x = r - r_p \ll 1$), we can rewrite the diffusion equation as

$$\frac{\partial \Sigma}{\partial t} = 3\nu_p \frac{\partial^2 \Sigma}{\partial x^2}. \quad (\text{A2})$$

Under the following initial and boundary conditions:

$$\Sigma(x, t = 0) = \Sigma_{\text{un}}, \quad (\text{A3})$$

$$\Sigma(x = 0, t) = 0, \quad (\text{A4})$$

we obtain the exact solution (e.g., Landau & Lifshitz 1987):

$$\Sigma(x, t) = \Sigma_{\text{un}} \operatorname{erf} \left(\frac{x}{2\sqrt{3\nu_p t}} \right), \quad (\text{A5})$$

where Σ_{un} is a constant.

Since the disk mass reduced from the initial condition equals to the mass sunk into the boundary at $x = 0$, we have

$$\begin{aligned} \int_0^t F(t') dt' &= 2\pi r_p \int_0^\infty (\Sigma_{\text{un}} - \Sigma(x, t)) dx \\ &= 2\pi r_p \Sigma_{\text{un}} \frac{2\sqrt{3\nu_p t}}{\sqrt{\pi}}, \end{aligned} \quad (\text{A6})$$

where $F(t)$ is mass flux toward $x = 0$ from $x > 0$, and we use a mathematical formula: $\int_0^\infty \operatorname{erfc}(x) dx = 1/\sqrt{\pi}$. Differentiating Equation (A6) with respect to time yields the mass accretion rate to the boundary $x = 0$ as a function of time:

$$F(t) = 2\pi r_p \Sigma_{\text{un}} \sqrt{\frac{3\nu_p}{\pi t}}. \quad (\text{A7})$$

B. A solution of a steady accretion disk with a mass sink to an embedded planet

Lubow & D'Angelo (2006) obtained the radial gas distribution of a steady viscous accretion disk with a mass sink by a planet and showed that the mass sink causes a gas depletion in a wide region, but did not give a detailed derivation of it. Here, we present the derivation the solution of the surface density distribution in such a case.

In an accretion disk, the radial angular momentum flux F_J is given by (Lynden-Bell & Pringle 1974)

$$F_J = jF_M + 3\pi r^2 \nu \Sigma \Omega, \quad (\text{B1})$$

where F_M is the radial mass flux and the specific angular momentum j is given by $r^2\Omega$. For Ω , the Keplerian rotation is assumed. Thus, for given (constant) mass flux and angular momentum flux, the surface density of the quasi-steady disk is expressed as

$$\Sigma(r) = \frac{-F_M + F_J/j(r)}{3\pi\nu(r)}. \quad (\text{B2})$$

We here consider an accretion disk having a mass sink with the rate of \dot{M}_p at $r = r_p$ due of the accretion onto the planet. The disk angular momentum sinks into the planet with the rate of $j(r_p)\dot{M}_p$. Then the mass and angular momentum fluxes are discontinuous at r_p and given by

$$F_M = \begin{cases} -(\dot{M}_* + \dot{M}_p) & (r > r_p), \\ -\dot{M}_* & (r < r_p), \end{cases} \quad (\text{B3})$$

and

$$F_J = \begin{cases} -(j_*\dot{M}_* + j_p\dot{M}_p) & (r > r_p), \\ -j_*\dot{M}_* & (r < r_p), \end{cases} \quad (\text{B4})$$

where \dot{M}_* is the mass accretion rate onto the central star and r_* is the radius of the inner disk edge. The specific angular momenta j_p and j_* are the values at r_p and r_* , respectively. Note that the sum $\dot{M}_p + \dot{M}_*$ is equal to the global accretion rate $\dot{M}_{\text{d,global}}$. The negative fluxes indicate the inward transport of the disk mass and angular momentum. Substituting Equations (B3) and (B4) into (B2), we obtain

$$\Sigma(r) = \begin{cases} \frac{\dot{M}_*}{3\pi\nu} \left(1 - \sqrt{\frac{r_*}{r}}\right) + \frac{\dot{M}_p}{3\pi\nu} \left(1 - \sqrt{\frac{r_p}{r}}\right) & \text{for } r > r_p, \\ \frac{\dot{M}_*}{3\pi\nu} \left(1 - \sqrt{\frac{r_*}{r}}\right) & \text{for } r < r_p. \end{cases} \quad (\text{B5})$$

The ratio \dot{M}_*/\dot{M}_p is determined by the accretion formula of Equation (7). From Equation (B5), we obtain

$$\Sigma(r_p) = \frac{\dot{M}_*}{3\pi\nu_p}, \quad (\text{B6})$$

where we omitted the term of $\sqrt{r_*/r_p}$. This approximation would be valid for a planet with $r_p \gtrsim 1\text{AU}$ since r_* would be less than 0.1AU . Note that the solution given by Lubow & D'Angelo (2006) does not assume that $r_* \ll r_p$. From Equations (7), (9) and (B6), we obtain

$$\dot{M}_p = \frac{D'}{3\pi\nu_p} \dot{M}_*, \quad (\text{B7})$$

where D' is defined by

$$D' = \frac{1}{0.034K + 1} D, \quad (\text{B8})$$

$\nu_p = \nu(r_p)$, and we equate $\Sigma(r_p)$ with Σ_{un} in Equation (9). Since the ratio $D'/3\pi\nu_p$ is equal to $\dot{M}_{p,\text{hydro}}/\dot{M}_{\text{d,global}}$ by definition, the ratio is given by Equation (16):

$$\frac{D'}{3\pi\nu_p} = 0.90 \left(\frac{M_p}{M_*} \right)^{-2/3} \left(\frac{h_p}{r_p} \right) = 4.5 \left(\frac{M_p}{M_J} \right)^{-2/3} \left(\frac{h_p/r_p}{0.05} \right). \quad (\text{B9})$$

Noting $\dot{M}_p + \dot{M}_* = \dot{M}_{\text{d,global}}$ and using Equation (B7), we obtain the accretion rates as

$$\dot{M}_p = \frac{D'/3\pi\nu_p}{1 + D'/3\pi\nu_p} \dot{M}_{\text{d,global}}, \quad \dot{M}_* = \frac{1}{1 + D'/3\pi\nu_p} \dot{M}_{\text{d,global}}. \quad (\text{B10})$$

Substituting Equation (B10) into (B5), we finally obtain the expression of the surface density of the disk with a mass sink of the planetary gas capture as

$$\Sigma(r) = \begin{cases} \frac{\dot{M}_{\text{d,global}}}{3\pi\nu(1 + D'/3\pi\nu_p)} \left[\left(1 - \sqrt{\frac{r_*}{r}} \right) + \frac{D'}{3\pi\nu_p} \left(1 - \sqrt{\frac{r_p}{r}} \right) \right] & \text{for } r > r_p, \\ \frac{\dot{M}_{\text{d,global}}}{3\pi\nu(1 + D'/3\pi\nu_p)} \left(1 - \sqrt{\frac{r_*}{r}} \right) & \text{for } r < r_p. \end{cases} \quad (\text{B11})$$

From the expression, the additional gas depletion factor due to the gas capture is given by $(1 + D'/3\pi\nu_p)^{-1}$, which is approximately equal to Equation (22) in the text. In Figure 10 we plot the obtained surface density distribution for a typical case. In the vicinity of the planet, the gap, which is an additional gas depletion due to the gravitational torque from the planet, should also exist. Even though the obtained surface density does not show this gap, the effect of the gap is included in this formulation through the parameter D' of Equation (B8).

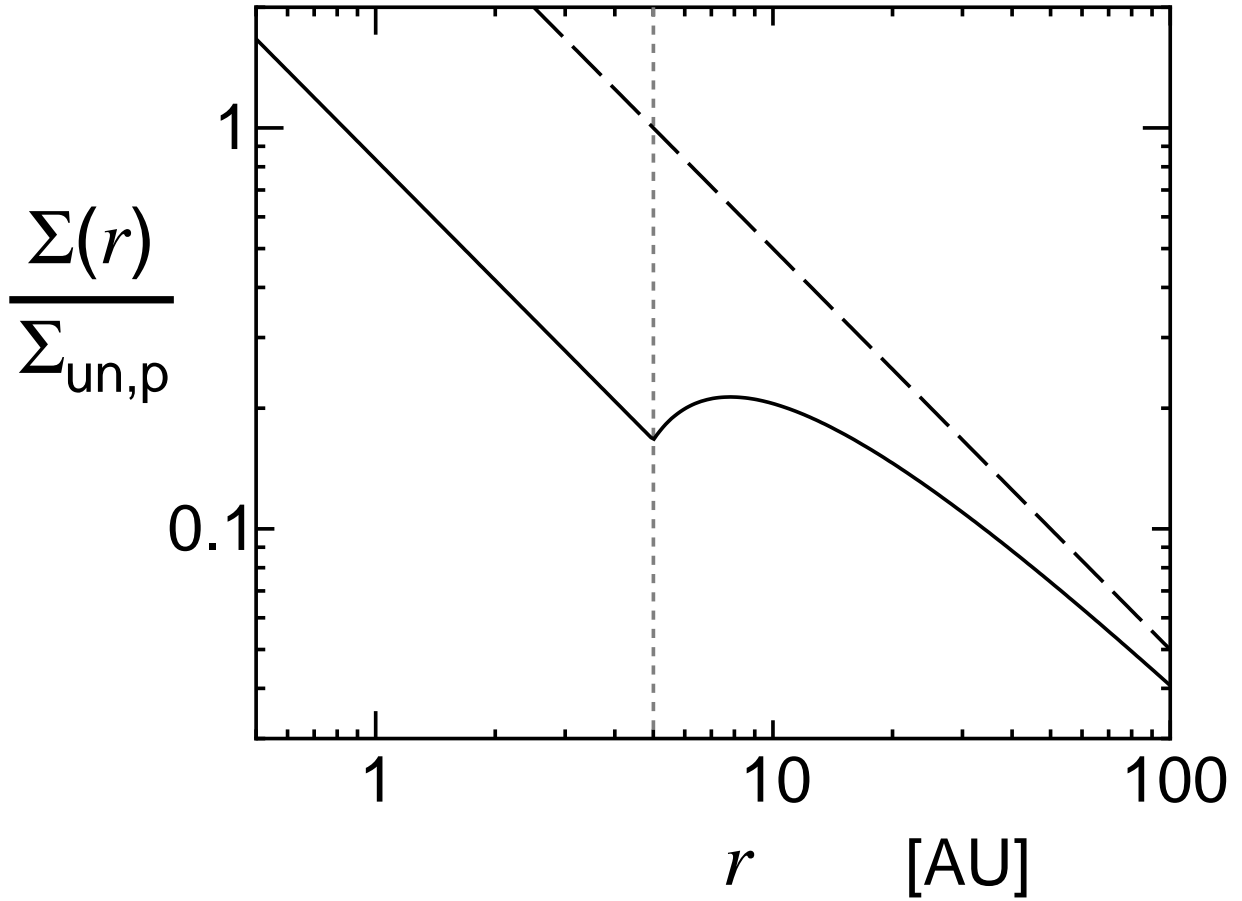


Fig. 10.— An example of the surface density distribution of the disk with a mass sink of the planetary gas capture (the solid line). The planet is located at 5AU (the vertical gray dotted line). The ratio $D/3\pi\nu_p$ is set to be 5. It is also assumed that $r \gg r_*$. The unperturbed surface density Σ_{un} is also plotted by the dashed line for comparison. Because of the planetary gas capture, the gas surface density is further depleted and an inner hole is formed.

REFERENCES

- Alexander, R., Pascucci, I., Andrews, S., Armitage, P., & Cieza, L. 2014, Protostars and Planets VI, Henrik Beuther, Ralf S. Klessen, Cornelis P. Dullemond, and Thomas Henning (eds.), University of Arizona Press, Tucson, 914 pp., p.475-496
- Armitage, P. J. 2007, *ApJ*, 665, 1381
- Baraffe, I., Chabrier, G., Fortney, J., & Sotin, C. 2014, Protostars and Planets VI, Henrik Beuther, Ralf S. Klessen, Cornelis P. Dullemond, and Thomas Henning (eds.), University of Arizona Press, Tucson, 914 pp., p.763-786
- Benz, W., Ida, S., Alibert, Y., Lin, D., & Mordasini, C. 2014, Protostars and Planets VI, Henrik Beuther, Ralf S. Klessen, Cornelis P. Dullemond, and Thomas Henning (eds.), University of Arizona Press, Tucson, 914 pp., p.691-713
- Bodenheimer, P., & Pollack, J. B. 1986, *Icarus*, 67, 391
- Clarke, C. J., Gendrin, A., & Sotomayer, M. 2001, *MNRAS*, 328, 485
- Crida, A., Morbidelli, A., & Masset, F. 2006, *Icarus*, 181, 587
- Daisaka, J. K., Tanaka, H., & Ida, S. 2006, *Icarus*, 185, 492
- D’Angelo, G., Kley, W., & Henning, T. 2003, *ApJ*, 586, 540
- Duffell, P. C., & MacFadyen A. I. 2013, *ApJ*, 769, 41
- Duffell, P. C., Haiman, Z., & MacFadyen, A. I., D’Orazio D. J., & Farris, B. D. 2014, *ApJ*, 792 10
- Dürmann, C., & Kley, W. 2015, *A&A*, 574, A52
- Elmegreen B. G. 1978, *Moon Planets*, 19, 261
- Fung, J., Shi, J.-M., & Chiang, E., *ApJ*, 782, 88
- Gorti, U, Dullemond, P., & Hollenbach, D. 2009, *ApJ*, 705, 1237
- Gressel, O., Nelson, R. P., Turner, N. J., & Ziegler, U. 2013, *ApJ*, 779, 59
- Hartmann, L., Calvet, N., Gullbring, E., & D’Alessio, P. 1998, *ApJ*, 495, 385
- Hasegawa, Y. & Ida, S. 2013, *ApJ*, 774, 146

- Hayashi, C., Nakazawa, K., & Nakagawa, Y. 1985, In *Protostars and Planets II*, eds. D. C. Black and M. S. Matthews, Univ. of Arizona Press, 1100
- Hollenbach, D., Johnstone, D., Lizano, S., & Shu, F. 1994, *ApJ*, 428, 654
- Horedt, G. P. 1978, *A&A*, 64, 173
- Hubickyj, O., Bodenheimer, P., & Lissauer, J. J. 2005, *Icarus*, 179, 415
- Ida, S., & Lin, D. N. C. 2004, *ApJ*, 604, 388
- Ida, S., & Lin, D. N. C. 2008, *ApJ*, 673, 487
- Ida, S., & Lin, D. N. C. 2008, *ApJ*, 685, 584
- Ida, S., Lin, D. N. C., & Nagasawa, M. 2013, *ApJ*, 775, 42
- Ikoma, M., Nakazawa, K., & Emori, H. 2000, *ApJ*, 537, 1013
- Kanagawa, K. D., Muto, T., Tanaka, H., Tanigawa, T., & Takeuchi, T. 2015, *MNRAS*, 448, 994
- Kanagawa, K. D., Tanaka, H., Muto, T., Tanigawa, T., Takeuchi, T., Tsukagoshi, T., & Momose, M. 2015, *ApJ*, 806, L15
- Keith S. L., & Wardle, M. 2015, *MNRAS*, 451, 1104
- Lin, D. N. C., & Papaloizou, J. 1986, *ApJ*, 309, 846
- Lin, D. N. C., & Papaloizou, J. 1993, *Protostars and planets III*, 749
- Lubow, S., H. & D'Angelo, G. 2006, *ApJ*, 641, 526
- Lynden-Bell, D. & Pringle J. E. 1974, *MNRAS*, 168, 603
- Malik, M., Meru, F., Mayer, L., & Meyer, M. 2015, *ApJ*, 802, 56
- Matsuyama, I., Johnstone, D., & Hollenbach, D. 2009, *ApJ*, 700, 10
- Machida, N. M., Kokubo, E., Inutsuka, S., & Matsumoto, T. 2010, *MNRAS*, 405, 1227
- Mayor, M.; Marmier, M.; Lovis, C.; Udry, S.; Ségransan, D.; Pepe, F.; Benz, W.; Bertaux, J. -L.; Bouchy, F.; Dumusque, X.; Lo Curto, G.; Mordasini, C.; Queloz, D.; Santos, N. C. 2011, *arXiv:1109.2497*
- Mizuno, H. 1980, *Prog. Theor. Phys.*, 64, 544

- Mordasini, C., Alibert, Y., Benz, W. 2009, A&A, 501, 1139
- Mordasini, C., Alibert, Y., Klahr, H., & Henning, T. 2012, A&A, 547, A111
- Mordasini, C., Alibert, Y., Benz, W., Klahr, H., & Henning, T. 2012, A&A, 541, 97
- Mordasini, C., Alibert, Y., Klahr, H., & Henning, T. 2012, A&A, 547, A112
- Owen, J. E., Clarke, C. J., & Ercolano, B. 2012, MNRAS, 422, 1880
- Pollack, J. B., Hubickyj, O., Bodenheimer, P., Lissauer, J. J., Podolak, M., & Greenzweig, Y. 1996, Icarus, 124, 62
- Landau, L. D., & Lifshitz, E. M. 1987, Fluid Mechanics, Second edition, U.S.S.R. Academy of Sciences
- Shakura, N. I., & Sunyaev, R. A. 1973, A&A, 24, 337
- Suzuki, T. K., & Inutsuka, S. 2009, ApJ, 691, L49
- Suzuki, T. K., & Inutsuka, S. 2014, ApJ, 784, 121
- Tanaka, H., Takeuchi, T., & Ward, W. R. 2002, ApJ, 565, 1257
- Tanigawa, T., & Watanabe, S. 2002, ApJ, 586, 506
- Tanigawa, T., & Ikoma, M. 2007, ApJ, 667, 557 (TI07)
- Tanigawa, T., Ohtsuki, K., & Machida, M. N. 2012, ApJ, 747, 47
- Williams, J. P., & Cieza, L. A. 2011, ARA&A, 49, 67